

Experiments and Simulations on A Metamaterial Based Ultrasonic Scanner

by

Fahri Erinc HIZIR

B.S. Mechanical Engineering, Middle East Technical University, 2008
M.S. Mechanical and Nuclear Engineering, Pennsylvania State University, 2010

Submitted to the Department of Mechanical Engineering
in partial fulfillment of the requirement for the degree of

Master of Science in Mechanical Engineering

at the

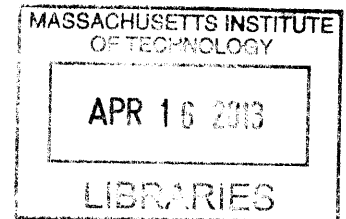
Massachusetts Institute of Technology

February 2013


©2013 Massachusetts Institute of Technology. All rights reserved.

The author hereby grants to MIT permission to reproduce and to distribute publicly
paper and electronic copies of this thesis document in whole or in part in any
medium known or hereafter created.


ARCHIVES



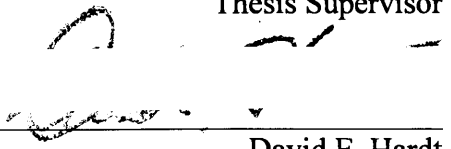
Signature of Author:


Department of Mechanical Engineering
22 January 2013

Certified by:


Nicholas X. Fang
d'Arbelloff Career Development Associate Professor
Thesis Supervisor

Accepted by:


David E. Hardt
Ralph E. and Eloise F. Cross Professor of Mechanical Engineering
Chairman, Committee for Graduate Students

“Hayatta en hakiki mürşit ilimdir, fendir.”

Mustafa Kemal Atatürk

Experiments and Simulations on A Metamaterial Based Ultrasonic Scanner

By

Fahri Erinc HIZIR

Submitted to the Department of Mechanical Engineering
on January 22, 2013 in Partial Fulfillment of the Requirements for
the Degree of Master of Science in
Mechanical Engineering

Abstract

Fingerprint scanning is one form of biometrics used to identify individuals. Ultrasonic fingerprint scanners use acoustic waves to obtain the fingerprint image and their performance is invariant to the surface conditions typically found on the finger surface due the ability of ultrasound to penetrate into sub-surfaces. This makes ultrasonic fingerprint scanning a superior technology to optical fingerprint imaging technologies [1].

In this thesis, we propose a new design of an ultrasonic fingerprint scanner, which has reduced complexity and lower cost of operation. The device uses a 1D array of transducers to generate focal spots under the finger surface and to scan the pressure field scattered by the finger ridges, while obtaining images. Integration of a metamaterial layer (an array of Helmholtz resonators) under the finger surface enables imaging features smaller than the diffraction limited spot. We expect such technique to increase the image resolution of the fingerprint scanner without need for an increase in the operating frequency or power consumption.

Simulation results presented in this thesis suggest that sub-wavelength acoustic focusing could be achieved over an array of Helmholtz resonators for high resolution acoustic imaging purposes. Underwater acoustic experiments performed to couple acoustic waves in the 40-60 KHz frequency range to an array of Helmholtz resonators are unsuccessful due to experimental limitations. Results of experiments involving two types of metamaterial and no metamaterial are compared. Furthermore, mathematical tools are developed which would help us better understand the propagation of acoustic signals through resonating structures. Our studies might provide quantitative information regarding resolution limits, and contribute to design guidelines for the construction of advanced metamaterial based ultrasonic imaging devices at MHz frequencies.

Thesis Supervisor : Nicholas X. Fang

Title : d'Arbeloff Career Development Associate Professor

[Left Blank]

Acknowledgements

I hereby want to acknowledge:

- My advisor Prof Nicholas X. Fang
- My family

[Left Blank]

Table of Contents

Acknowledgements.....	5
Table of Contents.....	7
List of Figures.....	9
List of Tables.....	12
Chapter 1 Introduction.....	14
1.1. Motivation.....	14
1.2. Thesis Outline.....	15
Chapter 2 An Overview of Fingerprint Imaging.....	17
2.1. Fingerprints.....	17
2.2. Brief History of Fingerprint Use.....	17
2.3. Analysis of Fingerprints.....	18
2.4. Detection of Fingerprints.....	18
2.4.1. Comparison Between Optical and Acoustic Fingerprint Scanners.....	19
2.5. The Need for an Improved Ultrasonic Fingerprint Scanner.....	21
Chapter 3 An Ultrasonic Fingerprint Scanner Based on Metamaterials.....	22
3.1. An Improved Ultrasonic Fingerprint Scanner Design.....	22
3.2. What are Evanescent Waves?.....	23
3.3. A Tool to Characterize Information Losses Due to Evanescent Waves.....	25
3.3.1. Description of the System.....	25
3.3.2. The Propagation Operator.....	26
3.3.3. Singular Value Decomposition.....	28
3.3.4. Meaning of the Singular Values.....	28
3.3.5. Simulations and Results.....	29
3.4. Role of Resonators.....	31
3.5. Helmholtz Resonators.....	33
3.6. Simulations Predicting the Performance of the Proposed Fingerprint Scanning Device.....	34
Chapter 4 Construction of the Ultrasonic Scanner.....	38
4.1. Components of the Experimental Setup.....	38
4.2. Preliminary Experimental Results.....	39
4.3. Prototype Ultrasonic Scanner.....	44
4.4. Experimental Results and Discussion.....	46
Chapter 5 Summary and Future Work.....	60
References.....	62

Appendix 66

5.1. Operational Conditions of Devices 66

List of Figures

Figure 1 Comparison of optical and ultrasonic fingerprint scanners. Images are adapted from reference [17] with permission from the author. 19

Figure 2 A high quality fingerprint image cannot be captured for an irregular ridge structure. Images are obtained from reference [19] with permission from the author. 20

Figure 3 Top and side views of the new ultrasonic fingerprint scanner design showing the components of the device such as Helmholtz resonators, transducers and the coupling liquid. 23

Figure 4 Propagating and evanescent waves obtained through simulations performed using COMSOL. In the simulations, magnitude of the wave vector is kept constant while increasing the k_x value so k_z becomes imaginary. For the evanescent wave shown in the figure, k_x/k is equal to 1.4. Simulations are done in water, with an acoustic source of frequency 60 KHz. The scale bar is 12 cm. Boundary conditions are defined as: left boundary - plane wave radiation, right boundary - matched boundary, top boundary - periodic condition, bottom boundary - periodic condition. Red color indicates a minimum in pressure and blue color indicates a maximum in pressure. 25

Figure 5 Acoustic focusing through a resonant structure over a finger surface 27

Figure 6 Set of equations which describe why time reversal symmetry is broken using singular values 29

Figure 7 Simulation domain used to obtain the transfer matrix..... 30

Figure 8 Singular value distribution of the transfer matrix for different separation distances between the transducer and microphone planes..... 30

Figure 9 Examples from the literature that show how resonating structures help prevent decay of evanescent waves [21, 22, 23] 32

Figure 10 Drawings of the Helmholtz resonator unit used in the ultrasonic fingerprint scanner: a) Circuit representation of the resonator, b) Dimensions of the Helmholtz resonator.... 34

Figure 11 Comparison of the size of the focal spot obtained with and without Helmholtz resonators. Results are obtained using Comsol. The medium of wave propagation is water. Frequency of the acoustic source is 60.5 KHz. Hard-wall boundary condition is used for the inner resonator surfaces, matched boundary condition is used for the side surfaces. Size of one unit cell is 3.175 mm in the drawings. Size of the scale bar is 48 mm. a) Simulation domain, b) Pressure distribution along a line passing through the center point of the resonator array and connecting middle points of the two edges, c) 3D representation of the pressure distribution in the simulation domain at the moment of acoustic focusing without Helmholtz resonators, d) 3D representation of the pressure distribution over the resonators at the moment of acoustic focusing with Helmholtz resonators..... 36

Figure 12 Simulations showing the increased resolution due to presence of the Helmholtz resonators. Results are obtained using Comsol. Size of the scale bar is 48 mm. The medium of wave propagation is water. Frequency of the acoustic source is 60.5 KHz. Hard-wall boundary condition is used for the inner resonator surfaces, matched boundary condition is used for the side surfaces. Size of the scale bar is 48 mm. a) Pressure distribution in the simulation domain at the moment of focusing with the scatter at the center (left) and the scatter shifted (right) without resonators, b) Pressure distribution in the simulation domain at the moment of focusing with the

	scatter at the at the center (left) and the scatter shifted (right) with resonators, c) Normalized pressure recorded by the detector for the case of no resonators in the simulation domain, d) Normalized pressure recorded by the detector with resonators in the simulation domain	37
Figure 13	Components of the experimental setup. a) Photograph showing the experimental setup, b) Diagram showing the connections between the different experimental components.	39
Figure 14	Experiments in the shallow water tank: a) Photograph of the experimental setup, b) Signal recorded by the hydrophone in a shallow water tank, when the transducer sends sinusoidal waves with frequency 60.5 KHz.	40
Figure 15	Simulation results showing the propagation of pressure waves through the experimental system, once an acoustic pulse is emitted in the 5 mm thick water layer. Arrow points in increasing time direction. Mediums of wave propagation are air, water, glass and aluminum from top to bottom. Frequency of the acoustic source is 60.5 KHz. Hard-wall boundary condition is used for the outer boundaries. Size of the scale bar is 2 cm.	41
Figure 16	Experiments performed in the plastic water tank. a) Drawing of the experimental setup with dimensions, b) Sample acoustic signal measured with the hydrophone	43
Figure 17	Prototype fingerprint imaging device. a) Drawing of the prototype fingerprint scanner, b) Simulations showing that a thin water layer can act as a waveguide. Mediums of wave propagation are air, water, and aluminum from top to bottom. Frequency of the acoustic source is 60.5 KHz. Hard-wall boundary condition is used for the aluminum boundaries, matched boundary condition is used for the outer boundaries. Size of the scale bar is 12 cm c) Photograph showing the experimental setup from the side, d) Photograph showing the experimental setup from the top.	43
Figure 18	Photographs of: a) Stainless steel block with dimensions 12 cm x 12 cm x 12 cm, b) Helmholtz resonator array placed on top of the resonator array.	44
Figure 19	Cross sectional view of the 3D-printed rubber setup for coupling acoustic waves to Helmholtz resonators.....	45
Figure 20	Schematic showing the two point source interference pattern. Wave crests are shown by thick lines and wave troughs are shown by thin lines. a) Demonstration of two sources (green), nodal points (blue), anti-nodal points (red). b) Demonstration of anti-nodal lines (red). Figure is adapted from reference [37].	47
Figure 21	Time domain signals measured for at the same hydrophone position for three different experimental configurations.	49
Figure 22	COMSOL simulations for acoustic focusing using two transducers: a) The simulation domain: Hard-wall boundary conditions are used for the inner resonator surfaces, matched boundary conditions are used for all the other (side) surfaces. Dimensions given on the figure have units of meters, b) Pressure distribution along a line joining the two acoustic sources with and without resonators, c) 3D representation of the pressure distribution in the simulation domain with resonators when the central interference region has minimum width at $t = 1.98347$ sec, d) 3D representation of the pressure distribution in the simulation domain without resonators when central interference region has minimum width at $t = 1.98347$ sec. The medium of wave propagation is water. The acoustic sources send five continuous sine waves with a frequency of 60.5 KHz. Each edge of the simulation domain is 47.6 mm in length. ..	50

Figure 23 Interference pattern recorded over the surface of the stainless steel block without Helmholtz resonators placed on it. Arrows point in increasing time direction. Medium is water, frequency of acoustic source is 60.5 KHz, scale bar is 12 mm, time of capture for each snapshot is indicated above it. For snapshots 3 – 8, $(\text{frequency}) \cdot (\Delta t) \approx (1\text{E}-6)(60.5\text{E}3)=0.06$ 53

Figure 24 Interference pattern recorded over the surface of the stainless steel block with Helmholtz resonators placed on it. Arrows point in increasing time direction. Medium is water, frequency of acoustic source is 60.5 KHz, scale bar is 12 mm, time of capture for each snapshot is indicated above it. For snapshots 2-7, $(\text{frequency}) \cdot (\Delta t) \approx (1\text{E}-6)(60.5\text{E}3)=0.06$ 54

Figure 25 Variation of pressure along the line connecting two spherical transducers over the metal block surface for different experimental configurations: no plate on the metal block, plate with holes on the metal block, resonator array on the metal block. One unit corresponds to 3.75 mm which is the spacing between the holes. All the pressure values are normalized by the maximum pressure value measured for the case of no plate on the metal block..... 55

Figure 26 Two point source interference pattern obtained using COMSOL without any Helmholtz resonators in the simulation domain. Medium is water, frequency of acoustic source is 60.5 KHz, size of the scale bar is 10 mm, time of capture for each snap shot is indicated above it..... 56

Figure 27 Two point source interference pattern obtained using COMSOL in the presence of Helmholtz resonators in the simulation domain. Medium is water, frequency of acoustic source is 60.5 KHz, size of the scale bar is 10 mm, time of capture for each snap shot is indicated above it..... 57

Figure 28 Snapshots showing the size of the constructive interference region at the center of the simulation domain with and without Helmholtz resonators at the same time steps. Medium is water, frequency of acoustic source is 60.5 KHz, each edge of the simulation domain is 47.6 mm in length. 58

Figure 29 Snapshots showing the propagation of acoustic signals through simulation domains with and without resonators. Medium is water, frequency of acoustic source is 60.5 KHz, each edge of the simulation domain is 47.6 mm in length. 59

List of Tables

Table 1 Distance the acoustic signals travel till reaching the hydrophone and expected time of arrival for the acoustic signal to reach the hydrophone, assuming speed of sound in water of 1482 m/s.	42
Table 2 Operating Conditions of the Devices Used in the Acoustic Focusing Experiments	66

[Left Blank]

Chapter 1 Introduction

1.1. Motivation

There are a number of examples in the literature of the use of ultrasonics to image fingerprints [2-4] for biometrics and diagnostics, most of which utilize fairly complex custom acoustic microscopes. However, there are not any working devices, either commercial off-the-shelf or in the development phase, which employ metamaterials for the application described above. Furthermore, to obtain the fingerprint image, conventional ultrasonic scanners use either 2D phased arrays, which increase manufacturing cost, or require the mechanical motion of a 1D array of transducers, which adds complexity to the scanner design [1-8].

In this study, we initiated a feasibility study regarding the potential of improving spatial resolution of a ultrasonic fingerprint scanner through the use of acoustic metamaterials together with our collaborators at Lincoln Laboratory [29]. The key idea of the proposed device is to reduce the number of transducers used for fingerprint scanning by placing the transducers on the perimeter of the scanner, as opposed to conventional ultrasonic scanners based on 2D array of piezoelectric devices, which leads to a simplified design and reduces the manufacturing cost. Survey of recent literature of the acoustic metamaterial layer suggests that, this simplified architecture could achieve increased resolution without need for an increase in the frequency of the acoustic signals used. This potentially could reduce the power consumption of the ultrasonic scanner during operation, and increase device fabrication yield (since less piezoelectric active elements are used on the chip).

Another motivation of this study is to study the feasibility of subwavelength acoustic imaging with acoustic metamaterials. Different metamaterial geometries, such as holey plates, have been previously used for sub-wavelength acoustic imaging [21]. In this thesis, we study the feasibility of Helmholtz resonators as acoustic imaging elements. Furthermore, we develop mathematical tools to better understand transmission of acoustic signals through resonating structures, which would help us design optimized metamaterial geometry for sub-wavelength acoustic imaging.

In summary, the following studies are performed in this thesis:

- An underwater acoustic system is developed to study acoustic signal transmission through resonant structures and investigate sub-wavelength acoustic imaging with acoustic metamaterials. The experimental results are compared with simulation results investigating acoustic signal transmission through an array of Helmholtz resonators [30].
- A comparison of acoustic wave propagation and acoustic focusing through three different experimental configurations is made: 1) A thin water layer acting as a waveguide over a stainless block surface, 2) a thin metal plate with holes immersed in a thin water layer, 3) an array of Helmholtz resonators placed in a thin water layer.
- Mathematical tools, which involve singular value decomposition, propagation operator and COMSOL simulations, are developed to better quantify loss of sub-diffraction-limited information of the transmitted signals during acoustic wave propagation.
- Simulations are done to better understand acoustic wave propagation through an array of Helmholtz resonators.

1.2. Thesis Outline

Chapter 2 makes an overview of fingerprint imaging starting with the history of fingerprint recognition. The chapter describes optical fingerprint imaging, the most common method of fingerprint imaging available in the market, and its disadvantages in comparison to ultrasonic fingerprint imaging justifying the need for the development of ultrasonic fingerprint sensors.

Chapter 3 describes the proposal of a new ultrasonic fingerprint scanner design with higher imaging resolution, reduced operational cost and a simplified design. Results of simulations are presented which confirm improved spatial resolution with the new design involving metamaterials. A simulation tool, with singular value decomposition for discrete number of transmitting and receiving transducers, is introduced which could be used to investigate how acoustic signals containing sub-diffraction limited information is decaying through regular imaging elements as well as resonant structures.

Chapter 4 introduces the components of the experimental system and explains the experimental effort performed to obtain acoustic focusing over an array of Helmholtz resonators in a water tank. A comparison of acoustic wave propagation and acoustic focusing through three different experimental configurations is made: 1) A thin water layer acting as a waveguide over a stainless block surface, 2) a thin metal plate with holes immersed in a thin water layer, 3) an array of Helmholtz resonators placed in a thin water layer. It also includes a discussion of the results and recommendations for future work.

Chapter 2 An Overview of Fingerprint Imaging

2.1. Fingerprints

Fingerprints are the unique patterns on the inside and the tips of fingers formed by the ridges of skin, also known as friction ridges, and the valleys between them [9]. Uniqueness of fingerprints, and the fact that they do not change during a person's life, form the basis for fingerprint analysis. Minute changes in local environment during fetal development determine uniqueness of the fingerprints. This enables differentiation of even identical twins, who are undistinguishable by DNA analysis, with fingerprint analysis [10].

Ridges vary in width from 100 μm , for very thin ridges, to 300 μm for thick ridges. The period of a ridge/valley cycle is about 500 μm in general. Most injuries to a finger such as superficial burns and cuts do not change the underlying ridge structure, and the original pattern is duplicated in the new skin which grows [17].

2.2. Brief History of Fingerprint Use

Nehemiah Grew published the first scientific paper to describe the ridge structure of the skin covering the fingers and palms in 1684 [11]. Marcello Malpighi made the first notes about the ridges, loops, and spirals of fingerprints in 1686 [12]. Mayer made the first detailed description of the anatomical formation of fingerprints, in which a number of fingerprint ridge characteristics were identified and characterized, in 1788 [17]. Starting in 1809, Thomas Bewick started using fingerprint as his trademark, which is one of the most important milestones in the history of fingerprints [17]. Purkinje proposed the first fingerprint classification scheme, which classified fingerprints into nine categories according to the ridge configurations in 1823 [17]. Henry Faulds recognized fingerprints as a means of personal identification and identified the first ever fingerprint in 1880 [13]. Sir Francis Galton conducted an extensive study on fingerprints and published the first book about the topic in 1888. Galton also introduced the minutiae features for comparing fingerprints and was the first to indicate that that no two prints are the same or the chance that the fingerprints of two individuals be the same is 1 in 64 billion [14]. Following Galton, in 1901, Sir Edward Henry developed the Henry Classification System, which

categorizes the ridge patterns into three groups as loops, whorls, and arches and forms the basis for print recognition [15]. Later, fingerprinting was introduced in prisons, army and widely used for identification by law enforcement.

Automation of the technology began when Federal Bureau of Investigation (FBI) wanted an identification system using fingerprints in 1969. To achieve this goal, the FBI worked in collaboration with the National Institute of Standards and Technology (NIST) to develop improved searching, matching and scanning processes. The best prototype developed in 1975 by the FBI used a capacitive scanning technique as its working basics and the minutiae technology, which is based on Galton's classification scheme. Further work on image compression, pattern matching and data acquisition is still being conducted [16].

2.3. Analysis of Fingerprints

Modern fingerprint analysis involves the use of computer algorithms to determine the similarity between a fingerprint and the images stored in a database by comparing ridges, bifurcations and their relative locations [6]. Analysis is usually performed on multiple levels starting from a coarse level to identify a type of fingerprint, and then narrowing down to identify more and more details until a match is found. Initially, the fingerprint analysis software identifies a set number of similarity points, this number being determined by the software used, where generally up to 90 points are compared. Following the identification of a specific number of features, a template of the scanned fingerprint is formed, which is subsequently compared to the templates stored in the computer to determine if the fingerprint has a match. Limiting the number of characteristics to be compared speeds up the matching process, but also leads to reduced accuracy, when an inadequate number of characteristics are used [16].

2.4. Detection of Fingerprints

The acquisition of fingerprints can be performed in two different ways, the ink-technique and live scanning. For the first method, which is mainly used in forensics, the subject's fingers are smeared with black ink and pressed or rolled on a paper card; the card is then scanned by using a general purpose scanner, producing a digital image. The live-scan fingerprint sensing method is generally used for authentication purposes in security applications.

Almost all the existing fingerprint sensors belong to one of the following three families: optical, solid-state, and ultrasound [17]. Working mechanism of optical scanners and the factors that limit their performance are described below. Later ultrasonic fingerprint scanners and their superior aspects in comparison to optical fingerprint scanners are explained to justify the reason why an improved ultrasonic fingerprint imaging device is constructed in this thesis.

2.4.1. Comparison Between Optical and Acoustic Fingerprint Scanners

Optical fingerprint scanning based on frustrated total internal reflection is the oldest and most commonly used live-scan acquisition technique today. As the finger touches the top side of a glass/plastic prism, the ridges are in optical contact with the prism surface, but the valleys remain at a certain distance (Figure 1). The left side of the prism is typically illuminated by diffused light (an array of light-emitting diodes or a film of planar light). The light entering the prism is reflected at the valleys, and randomly scattered (absorbed) at the ridges. The lack of reflection allows the ridges (which appear dark in the image) to be discriminated from the valleys (appearing bright). The light rays exit from the right side of the prism and are focused through a lens onto a CCD or CMOS image sensor [17].

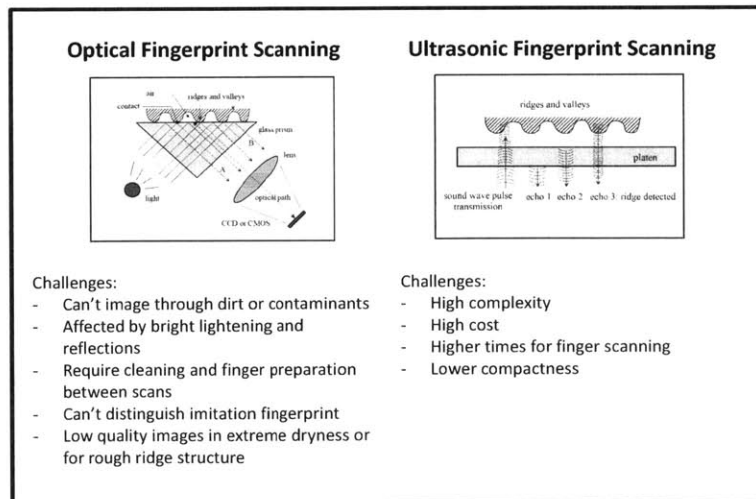


Figure 1 Comparison of optical and ultrasonic fingerprint scanners. Images are adapted from reference [17] with permission from the author.

As frustrated total internal reflection occurs, the light breaks out of the surface of the prism at a distance that is well defined and known as the depth of penetration, which is a function of the wavelength of the light used and indices of refraction involved. If the fingerprint ridge does not fall within the depth of penetration, then it will not be imaged (Figure 2). This will occur if:

- the contaminant or oil layer on the finger is greater than the depth of penetration
- extreme dryness or rough ridge structure causes air pockets between the finger and the platen that are greater than depth of penetration (Figure 2) [19].

Factors described above limit the quality of an optical image captured for a very dry or oily finger, in very low humidity, if the ridge structure is irregular or the scanner platen becomes coated with dirt.

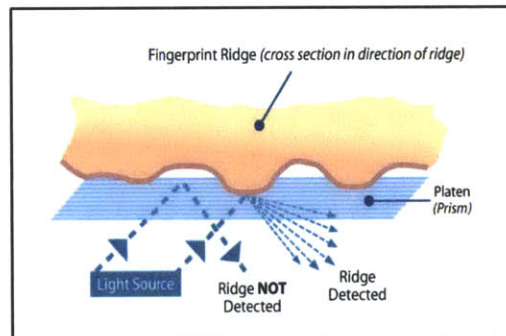


Figure 2 A high quality fingerprint image cannot be captured for an irregular ridge structure. Images are obtained from reference [19] with permission from the author.

On the other hand, performance of ultrasonic fingerprint scanners is not limited by the factors described above, since its working mechanism is based on sending acoustic signals towards the fingertip and capturing the echo signal (Figure 2). The echo signal is used to compute the range (depth) image of the fingerprint and, subsequently, the ridge structure itself. The ultrasound sensor has two main components: a transmitter, which generates short acoustic pulses, and a receiver, which detects the responses obtained when these pulses bounce off fingerprint surface [17]. Because ultrasound has the ability to penetrate many materials, its

performance is invariant to the surface conditions typically found on the finger. Hence, superior to optical fingerprint imaging devices, ultrasonic fingerprint scanners:

- can read through dirt, oil, grease, ink, and other contaminants commonly found on human fingers;
- can operate even in total darkness, so they are not affected by bright lighting, reflections, or glare, as is the case with optical systems;
- require no cleaning or finger preparation between scans;
- can distinguish an imitation fingerprint from a real one.

2.5. The Need for an Improved Ultrasonic Fingerprint Scanner

Working of current ultrasonic fingerprint imaging devices are based on 2D transducer arrays, which are capable of sending ultrasonic waves to desired locations on the finger surface and collecting the reflections back. However, cost of 2D transducer arrays is high and patterning of piezoelectric-based transducer devices is not standard. Unlike digital optical cameras (currently used in fingerprint imaging), for 2D ultrasonic cameras typical cost is around \$10,000 or above. Therefore, there is a need to develop the current ultrasonic fingerprint imaging technology and obtain more cost-efficient devices [5, 6, 7, 8].

In this thesis, a more cost-efficient ultrasonic fingerprint scanner with simplified design, lower power consumption and improved resolution is proposed to address the above need upon the request of our collaborators in Lincoln Laboratory.

Chapter 3 An Ultrasonic Fingerprint Scanner Based on Metamaterials

3.1. An Improved Ultrasonic Fingerprint Scanner Design

In this section, the design of an improved ultrasonic fingerprint scanner is explained. The new fingerprint scanner:

- replaces the 2D transducer array with a 1D set of transducers. This simplifies the design and makes it more cost-efficient.
- does not require motion of the 1D transducer array to scan the fingerprint. This reduces complexity due to moving components.
- uses a layer of metamaterial (an array of Helmholtz resonators) to achieve high resolution without any need for an increase in the frequency of the signals emitted by the transducers. Use of lower frequency values for imaging reduces power consumption during device operation.
- operates in water, which could be replaced by a different fluid that has impedance value close to that of the finger. This enables better coupling of acoustic waves to the finger ridges and helps imaging deeper into the finger.

A schematic drawing of the fingerprint scanner is shown in Figure 3. We propose to deposit a 1D transducer array on a hollow rectangle, which is capable of producing focal spots in the region it encloses. The fingerprint pattern to be imaged, is placed inside the hollow rectangle surrounded by the transducer array. The focal spots act as imaging probes that interact with the fingerprint pattern. Images of fingerprints can be obtained by recording the pressure field scattered by the finger ridges with the same 1D transducer array.

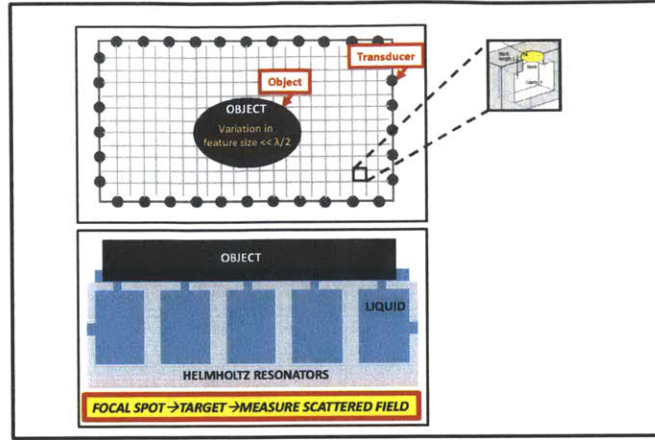


Figure 3 Top and side views of the new ultrasonic fingerprint scanner design showing the components of the device such as Helmholtz resonators, transducers and the coupling liquid.

An array of Helmholtz resonators placed inside the rectangular region (with a resonance frequency that matches the resonance frequency of the signals emitted by the transducer array) decreases the size of the focal spots obtained without any need for an increase in frequency by converting the evanescent acoustic waves released from the transducers to propagating ones.

3.2. What are Evanescent Waves?

Evanescent waves are near-field standing waves with an intensity that exhibits exponential decay with distance from the boundary at which the wave was formed [20]. To better understand evanescent waves, consider the two dimensional x-z space with waves travelling from a line source on the left-hand side towards a receiver on the right-hand side (Figure 4). The equation for the plane waves is given by

$$P(x, z, t) = P_0 e^{i(k_x x + k_z z - \omega t + \Phi)} \quad (1)$$

where ω is the angular frequency of the wave, Φ is the phase-shift of the wave, k_x and k_z are the x and z components of the wave vector determining the direction of propagation of the plane waves.

Magnitude of wave vector is fixed for waves with fixed frequency and a medium with constant properties. Magnitude of the wave vector is defined such that

$$\sqrt{k_x^2 + k_z^2} = \left\{ \frac{2\pi}{\lambda_0} \right\} = k_0 \quad (2)$$

For the case of plane propagating waves,

$$-k_0 \leq k_x \leq k_0 \quad (3)$$

$$-k_0 \leq k_z \leq k_0 \quad (4)$$

$$P(x, z, t) = P_0 e^{i(k_x x + k_z z - \omega t + \Phi)} \quad (5)$$

For the case of evanescent waves,

$$k_x \geq k_0 \quad (6)$$

and therefore k_z becomes imaginary (indicated by ik'_z). Hence, the equation for the evanescent wave becomes

$$P(x, z, t) = P_0 e^{i(k_x x - \omega t + \Phi) - k'_z z} \quad (7)$$

As can be seen in Figure 4 and as described in Equation 7, amplitude of the evanescent pressure waves decay exponentially, as the waves propagate away from the source location (Figure 4). Decay of the evanescent waves limits resolution in imaging, since evanescent waves carry information about sub-wavelength features of objects. The information carried by the evanescent waves can be recovered by preventing the decay of the evanescent waves using methods such as allowing no distance for evanescent waves to decay by placing the detector in the near-field of the source, using negative index media to amplify evanescent waves, converting evanescent waves to propagating waves by the use of resonating structures, coupling evanescent waves to resonating structures.

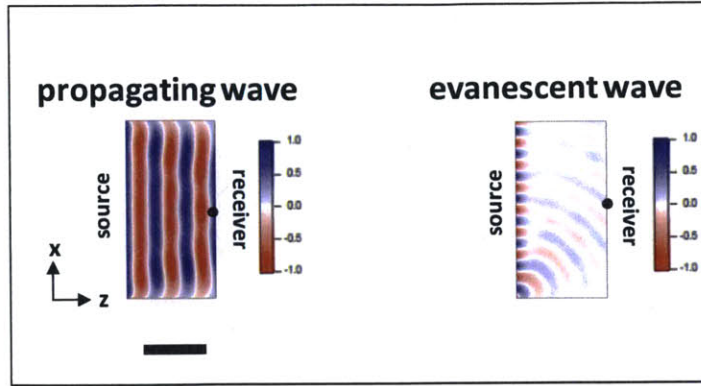


Figure 4 Propagating and evanescent waves obtained through simulations performed using COMSOL. In the simulations, magnitude of the wave vector is kept constant while increasing the k_x value so k_z becomes imaginary. For the evanescent wave shown in the figure, k_x/k is equal to 1.4. Simulations are done in water, with an acoustic source of frequency 60 KHz. The scale bar is 12 cm. Boundary conditions are defined as: left boundary - plane wave radiation, right boundary - matched boundary, top boundary - periodic condition, bottom boundary - periodic condition. Red color indicates a minimum in pressure and blue color indicates a maximum in pressure.

3.3. A Tool to Characterize Information Losses Due to Evanescent Waves

The above analysis of evanescent waves and spatial resolution is established based on continuous Fourier transform in the spatial domain. In the following sections, we introduce a method, which uses singular value decomposition of a matrix that represents the propagation operator that connect a discrete array of sources to an array of receivers, to better describe losses during acoustic signal transmission. An example is presented which demonstrates losses due to decay of evanescent waves.

3.3.1. Description of the System

Consider the 1D array of M transducers located at position \mathbf{r} which focus acoustic waves through a resonant structure at J points on the surface of a finger located at position \mathbf{r}_0 (Figure 5). The medium in which acoustic wave propagates, in this specific case, is composed of resonant structures such as Helmholtz resonators. Such medium, together with the array of transducers and

imaging points, can be thought of as a filter. The input signals to the filter are acoustic emission from the transducer elements and the output signals are the pressure signals measured at the control points on the finger surface. Such signal transfer involve losses of information: the contribution is a sum of decay of evanescent waves, finite number of transducers, absorption of acoustic energy through the medium of propagation etc. Such information loss through the abovementioned filter, lead to an increase in the size of the focal spot formed on the finger surface.

In the following sections it will be explained that losses of information taking place as signals propagate through the filter are related to the singular values of the transfer matrix representing the filter.

3.3.2. The Propagation Operator

Let $e_j(t)$, $1 \leq j \leq J$, be the input signals on the transducer array and $f_m(t)$, $1 \leq m \leq M$, be the received signals in the control domain. An impulse response, $h_{mj}(t)$, can be defined for each couple (m, j) comprising a control point and a transducer element. The impulse response $h_{mj}(t)$ is the signal received on the m^{th} control point when a temporal Dirac's function is applied on the j^{th} transducer.

The output signals $f_m(t)$, can be related to the input signals $e_j(t)$ by the following relation, where $*$ is a temporal convolution operator.

$$f_m = \sum_{j=1}^J h_{mj}(t) * e_j(t), 1 \leq m \leq M \quad (8)$$

A temporal Fourier transform of Equation (7) leads to the following relation:

$$F_m(\omega) = \sum_{j=1}^J H_{mj}(\omega) E_j(\omega), 1 \leq m \leq M \quad (9)$$

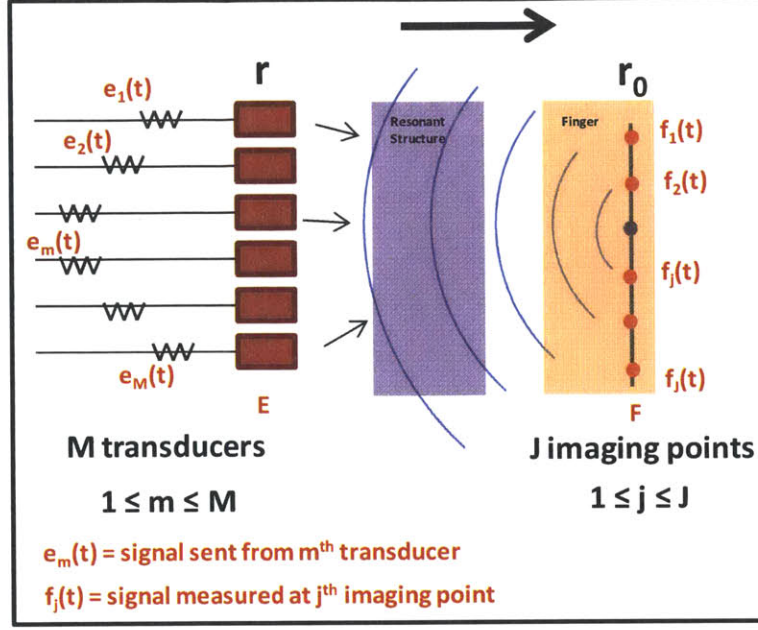


Figure 5 Acoustic focusing through a resonant structure over a finger surface

This equation drops down to the simplified matrix form:

$$F(\omega) = \mathbf{H}(\omega)E(\omega) \quad (10)$$

In this representation $E(\omega) = (E_j(\omega))_{1 \leq j \leq J}$ is the column vector of the Fourier transform of the transmitted signals and $F(\omega) = (F_m(\omega))_{1 \leq m \leq M}$ is the column vector of the Fourier transform of the received signals. The transfer matrix $\mathbf{H}(\omega) = (H_{mj}(\omega))_{1 \leq m \leq M, 1 \leq j \leq J}$ describes the propagation in the medium from the transducer array to the control points on the finger surface. Therefore it is called the propagation operator [28, 36]. Open form of the propagation operator is shown below.

$$\mathbf{H} = \begin{bmatrix} H_{e1f1} & H_{e2f1} & \dots & H_{eMf1} \\ H_{e1f2} & H_{e2f2} & \dots & H_{eMf2} \\ \dots & \dots & \dots & \dots \\ H_{e1fJ} & H_{e2fJ} & \dots & H_{eMfJ} \end{bmatrix} \quad (11)$$

3.3.3. Singular Value Decomposition

If H is an $m \times j$ matrix with complex entries, then H can be written using the so-called singular value decomposition as

$$H = UD V^H \quad (12)$$

where U is a $m \times j$ column-orthogonal matrix, and V is a $j \times j$ orthogonal matrix, V^H is the conjugate transpose of V , and D is a diagonal matrix whose elements are the singular values of the original matrix [26]. The singular values are always positive for a complex H matrix.

3.3.4. Meaning of the Singular Values

Singular values of the propagation operator are related to information loss in a system. Two examples of this relation are described in the paragraphs below.

In digital image processing, the compression of an image can be achieved by eliminating its zero singular values. The elimination of more singular values leads to a blurry image with lower quality and higher compression ratio [27].

As described by the set of equations in Figure 6, loss of information during a time reversal process (due to decay of evanescent waves, absorption in the medium, finite number of transducers, large spacing between the individual transducers or control points) can be quantified by the zero singular values of the propagation operator representing this system [28]. For a given pressure pattern F on the control points, the signal pattern required to be released from the array of transducers, E , can be calculated by taking the inverse of the propagation operator H and multiplying it with F . Since the H matrix is ill-conditioned, some of its singular values are neglected during the inversion process. Due to the neglected singular values, release of the calculated pressure pattern E from the array of transducers will not lead to the desired pressure pattern F on the control points. The singular values of the propagation operator represent information loss during the time reversal process and break down the time reversal symmetry.

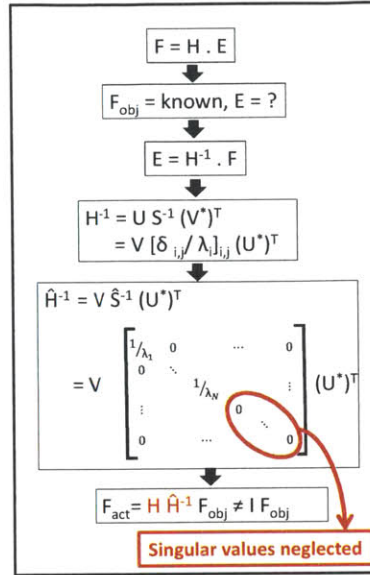


Figure 6 Set of equations which describe why time reversal symmetry is broken using singular values

3.3.5. Simulations and Results

Simulations are performed to obtain the propagation matrix using a 1D array of transducers and microphones in water. The singular value distribution of the propagation matrix is compared for different values of the spacing between the transducer and microphone planes to see the effect of the decay of evanescent waves on the singular value distribution.

In the simulations, length of each one of the 1D arrays is 4 cm (L and D), spacing between subsequent transducers and microphones is 0.4cm (a). Transfer matrices are obtained by sending pressure pulses from each transducer and recording the resulting pressure field with the microphone array. A comparison of the singular values for separation distances between the two planes (F) being 2 cm and 0.08 cm (much less than the wavelength) is shown in Figure 7.

Results show that for the case of spacing between the two planes being much less than the acoustic wavelength, the singular values are higher in magnitude (Figure 8). The increased magnitude of the singular values for this case is due to the prevention of the decay of the evanescent waves over shorter distances.

Extension of these simulations to include different resonator geometries could be useful in designing resonators that lead to minimal information loss during transmission of signals through resonating structures.

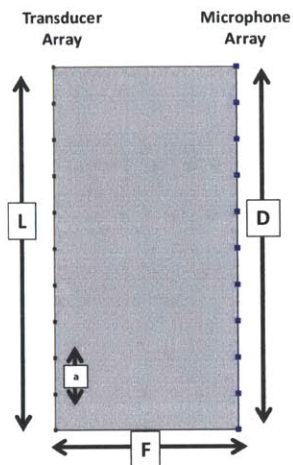


Figure 7 Simulation domain used to obtain the transfer matrix

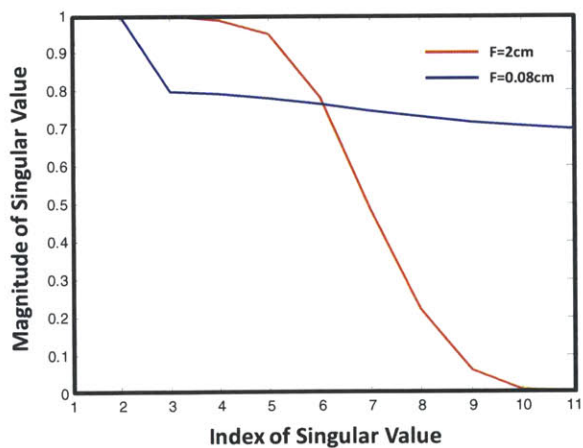


Figure 8 Singular value distribution of the transfer matrix for different separation distances between the transducer and microphone planes

3.4. Role of Resonators

Diffraction limits the size of a focal spot obtained by the interference of waves coming from different sources (transducers on the hollow rectangle in this specific case) [20]. This is due to the decay of evanescent waves, as they propagate from the source location towards the focal spot location. As described in several examples in the literature, some of which are summarized in Figure 9 [21, 22, 23], by placing resonating structures between the acoustic source and the focal spot location, the decay of the evanescent waves can be prevented. This enables obtaining focal spots with sizes smaller than what is predicted by the diffraction limit (half of the wavelength value).

Figure 9-a shows that when the frequency of an acoustic source in the shape of letter E is matched with the Fabry-Perot resonance frequency of a holey-material, the acoustic image transmitted to the opposite side of the holey-material contains features of dimension, $\lambda/50$, beating the diffraction limit [21]. The holey-material in this example is a 2D lens, which operates in air at a frequency of 2.18 KHz and has a thickness value of 158 mm (equal to one wavelength for the given frequency). Figure 9-b shows that when a pulse centered around 400 Hz is sent from the center of an ensemble of 7x7 soda cans with resonance frequency of 420 Hz, then the resulting pressure field is recorded by loudspeakers surrounding the source, the recording is time-reversed and played backwards, a focal spot of size $\lambda/8$ is obtained at the initial source location [22]. The reduced focal spot size obtained in the presence of soda cans is due to conversion of evanescent waves to propagating ones as the acoustic waves move over the resonating soda cans. Similarly, a focal spot beating the diffraction limit obtained by acoustic focusing over a Helmholtz resonator-based negative index media is shown in Figure 9-c [23]. The Helmholtz resonators used in this study have a resonance frequency of 60.5 KHz and acoustic focusing is achieved by combining two mediums: one with positive index and one with negative index. Amplification of the evanescent waves due to the negative index media is responsible for the sub-wavelength size of the focal spot.

Similar to the examples described above, in the new ultrasonic fingerprint scanner design, an array of resonating structures (Helmholtz resonators) are placed inside the 1D array of ultrasonic transducers (medium of wave propagation). The resonance frequency of the Helmholtz

resonators matches with the operating frequency of the fingerprint scanner. As the acoustic waves propagate from the source location towards the focal spot location, due to the existence of the resonators in the medium of wave propagation, evanescent waves are converted to propagating waves. This prevents the decay of evanescent waves and enables obtaining focal spots with reduced sizes, while keeping the frequency value the same, similar to the above examples. This leads to high resolution imaging at lower frequency values and reduces the power consumption of the fingerprint scanner during operation.

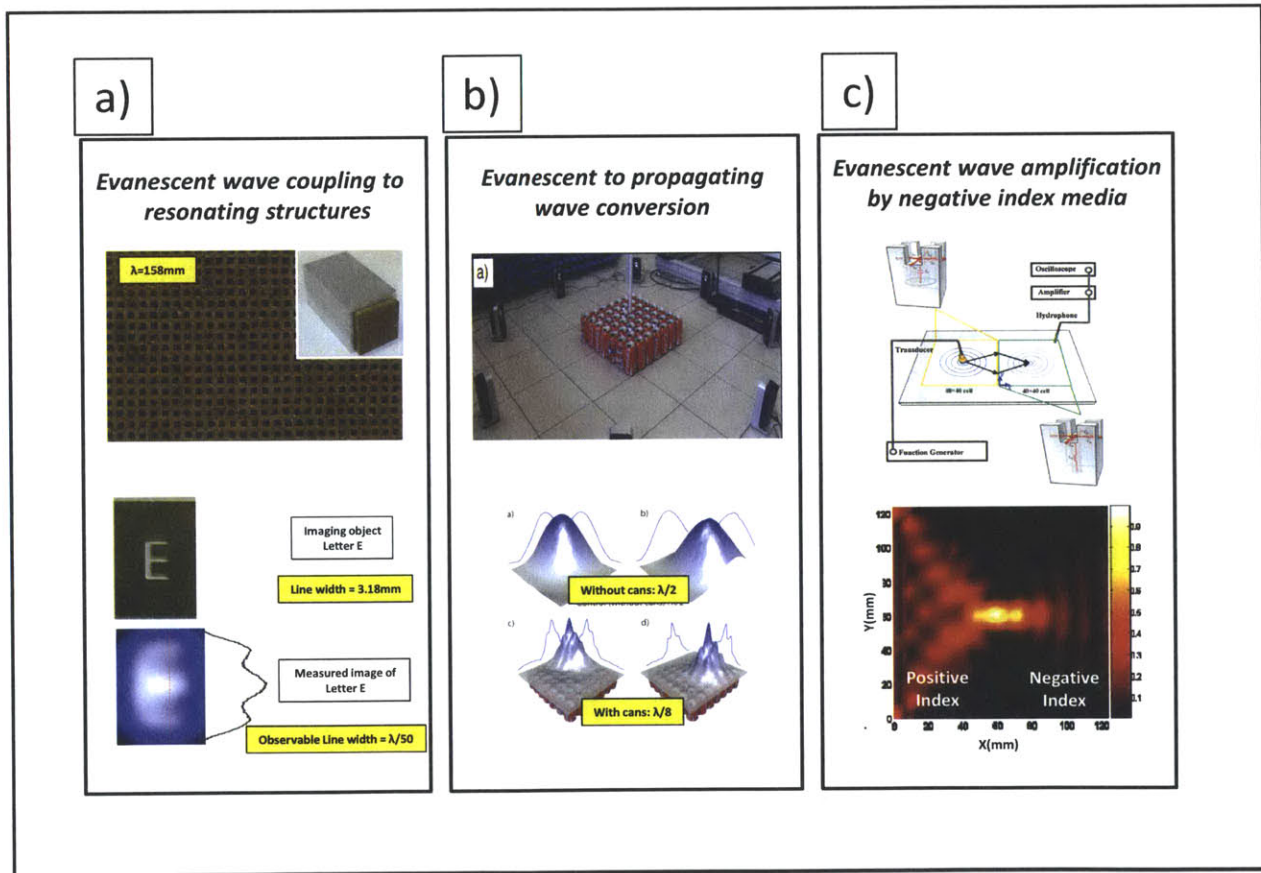


Figure 9 Examples from the literature that show how resonating structures help prevent decay of evanescent waves [21, 22, 23]

3.5. Helmholtz Resonators

Acoustic metamaterials are artificially fabricated materials designed to control, direct, and manipulate acoustic waves [25]. The building block of the ultrasonic metamaterial used in the ultrasonic fingerprint scanner, the Helmholtz resonator, consists of a cavity of known volume with rigid walls and a small hole in one side (Figure 10-a). Variation of the pressure inside the channel causes the plug of fluid in the hole to oscillate in and out, which leads to the adiabatic compression and rarefaction of the liquid enclosed in the cavity. Such a resonator is analogous to an inductor–capacitor circuit, where the enclosed cavity acts as a capacitor with capacitance $C \sim V/\rho c^2$, and the neck acts as the inductor ($L \sim \rho(L'/S)$) (Figure 10-a). In the symbolism used, V is the volume of the cavity, ρ is the density of the fluid, c is the sound speed in the fluid, L' is the effective length of the neck, and S is the cross-sectional area of the neck [24].

Since a Helmholtz resonator does not require standing waves to create a resonance, the dimension of each element can be made much smaller than the acoustic wavelength which is about 2.4 cm at a frequency of 60.5 KHz in water. For the Helmholtz resonator array used in the experiments, which is the same Helmholtz resonator structure with negative-index designed in our group for acoustic focusing experiments [23], the size of each Helmholtz resonator unit is 3.75 mm x 3.75 mm, and its resonance frequency is designed to be 60.5 KHz (Figure 10-b). Because the periodicity of the resonators is considerably smaller than the corresponding longitudinal wavelength in water, the ultrasonic metamaterial behaves as a homogenized medium.

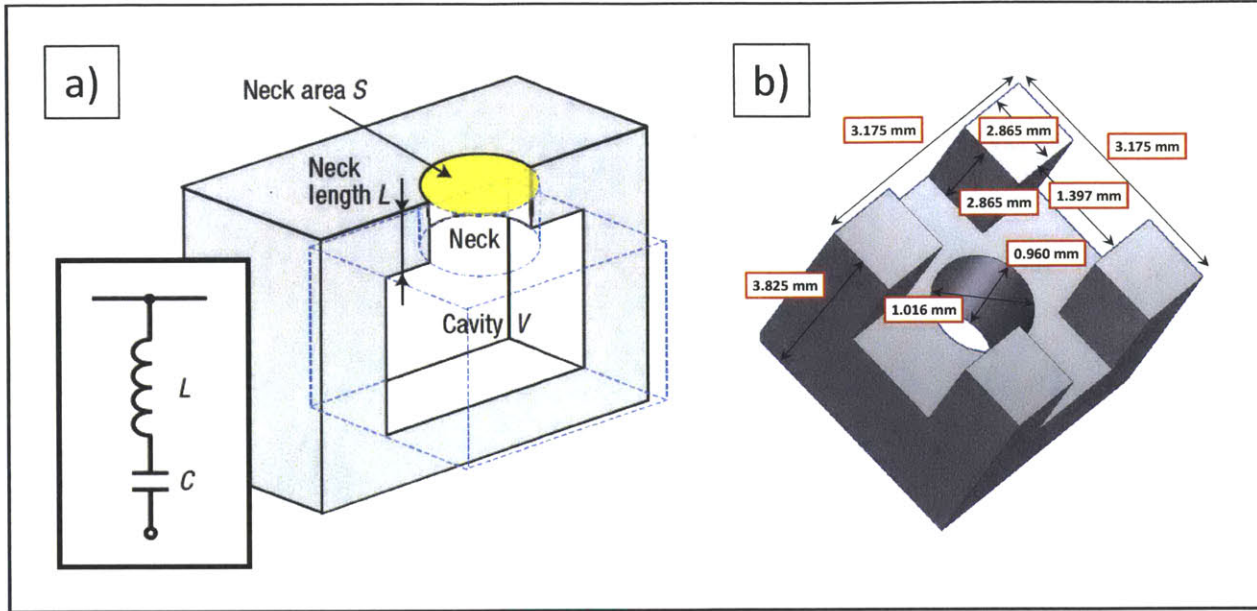


Figure 10 Drawings of the Helmholtz resonator unit used in the ultrasonic fingerprint scanner: a) Circuit representation of the resonator, b) Dimensions of the Helmholtz resonator

3.6. Simulations Predicting the Performance of the Proposed Fingerprint Scanning Device

The following simulations are performed by Dr Jun Xu with reduced number of transducers to verify that the proposed device will function as predicted, leading to increased resolution [30]. Another goal of the simulations is to better understand the propagation of acoustic signals through an array resonating structures (Helmholtz resonators in this specific example), which is an important topic of study in the field of wave propagation [31-34]. In the simulations, Gaussian pulses with a center frequency of 60.5 KHz are sent from four point sources placed at the four corners of an array of 15x15 Helmholtz resonators (Figure 11-a).

Figure 11 (b, c, d) shows the reduction in the size of the focal spot (full width at half maximum) obtained at the center of the resonator array from the half the wavelength value of 12 mm predicted by the diffraction limit to a value of 9 mm in the presence of the Helmholtz resonator array due to conversion of evanescent waves to propagating ones. This result confirms

that the Helmholtz resonators designed in our group for making an acoustic lens can also be used for obtaining focal spots beating the diffraction limit.

A second set of simulations are performed to understand the effect of the reduced spot size on the resolution of imaging. In these simulations, a cylindrical scatter made of PMMA, which is 3.2 mm in diameter and 2 mm in height, is placed on top of the resonator array (Figure 12-a,b). Gaussian pulses are sent from four corners of the resonator array as before. The resulting pressure field is measured with a detector placed at the center of the lower edge of the resonator array. The pressure fields recorded by the detector for two different cases: 1) PMMA scatter placed at the center of the resonator array, 2) PMMA scatter shifted 7.5mm (a shift which is less than the wavelength value) to the left, are compared with and without Helmholtz resonators in the simulation domain. Results indicate a 220% increase in the normalized pressure value recorded by the detector due to the shift of the scatter, when the array of resonators are included in the simulation domain compared to the case of no Helmholtz resonators. The prominent difference in the amplitude of the signal value measured by the detector confirms easier detection of the scatter (for a shift in its position less than the wavelength value) in the presence of the resonators (Figure 12-c,d).

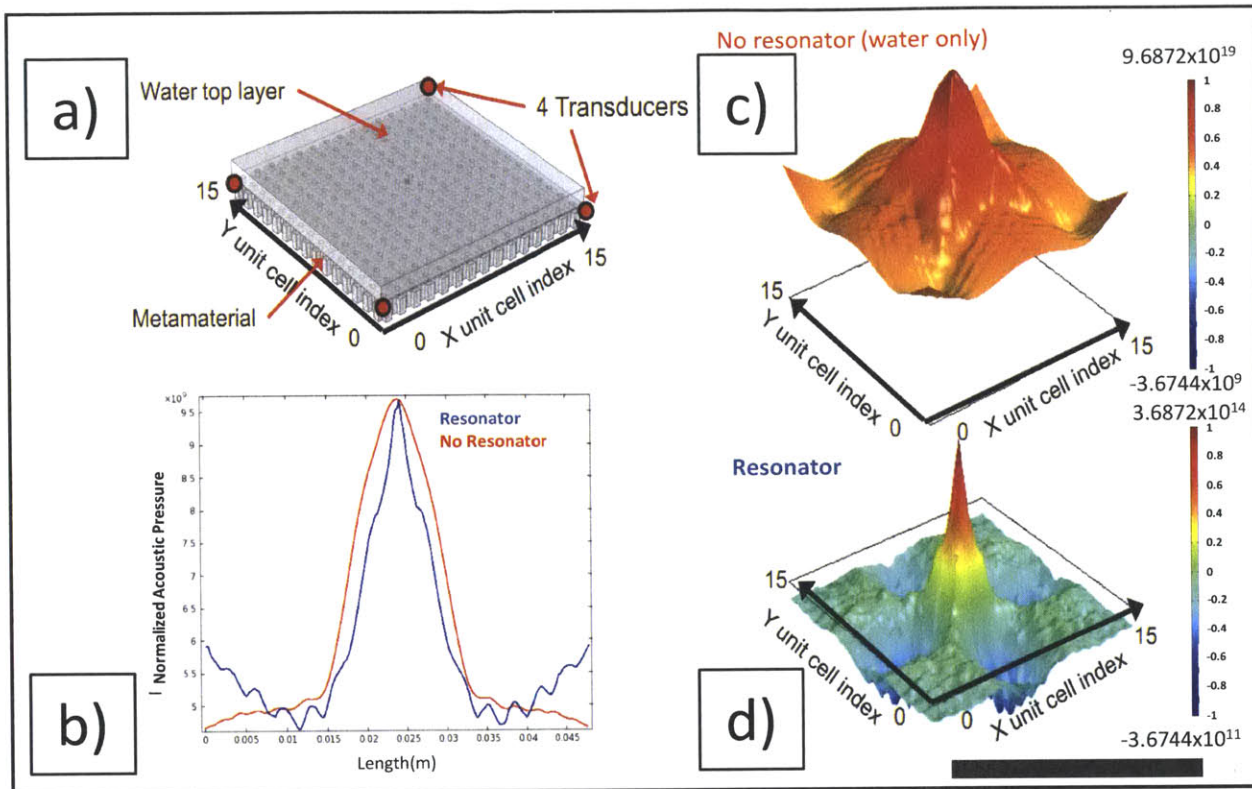


Figure 11 Comparison of the size of the focal spot obtained with and without Helmholtz resonators. Results are obtained using Comsol. The medium of wave propagation is water. Frequency of the acoustic source is 60.5 KHz. Hard-wall boundary condition is used for the inner resonator surfaces, matched boundary condition is used for the side surfaces. Size of one unit cell is 3.175 mm in the drawings. Size of the scale bar is 48 mm. a) Simulation domain, b) Pressure distribution along a line passing through the center point of the resonator array and connecting middle points of the two edges, c) 3D representation of the pressure distribution in the simulation domain at the moment of acoustic focusing without Helmholtz resonators, d) 3D representation of the pressure distribution over the resonators at the moment of acoustic focusing with Helmholtz resonators

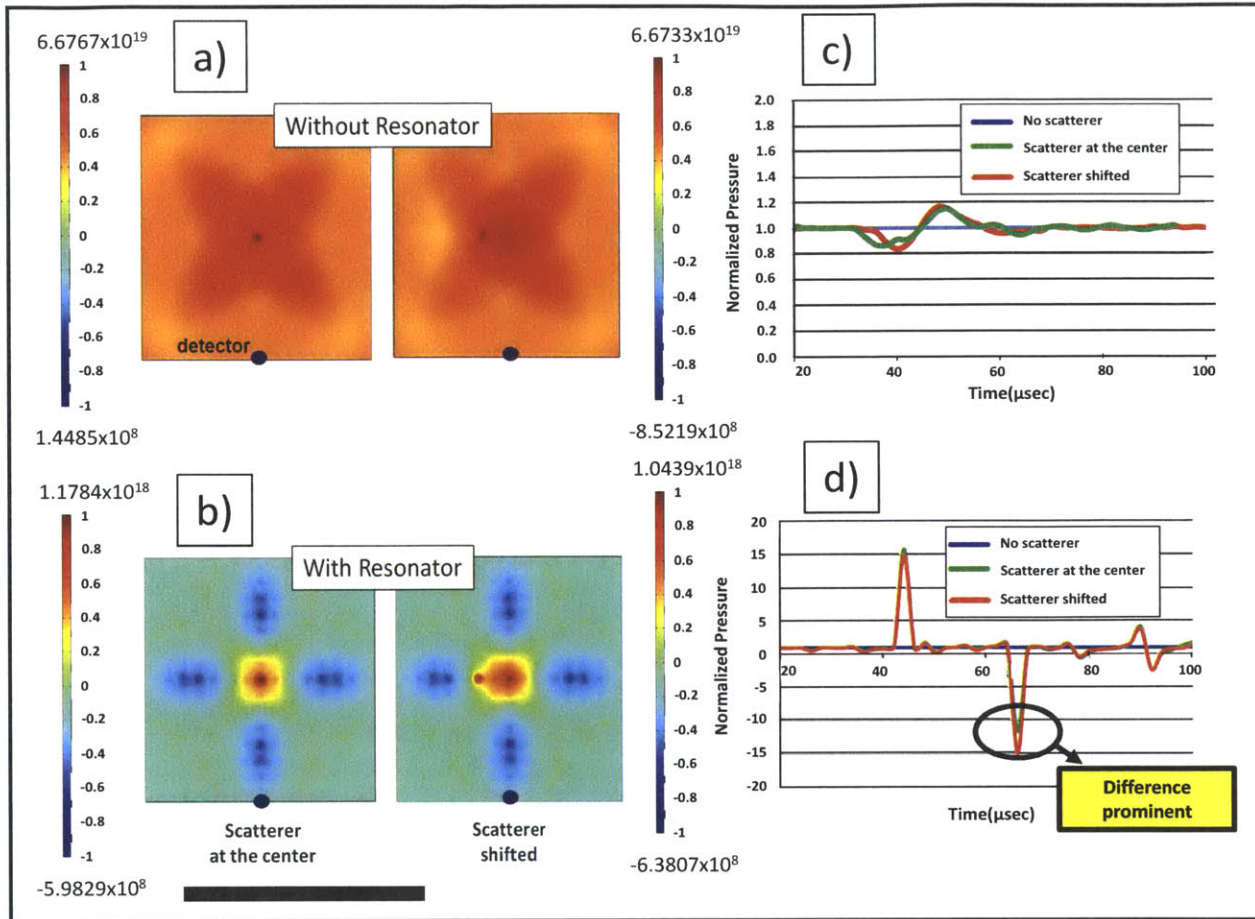


Figure 12 Simulations showing the increased resolution due to presence of the Helmholtz resonators. Results are obtained using Comsol. Size of the scale bar is 48 mm. The medium of wave propagation is water. Frequency of the acoustic source is 60.5 KHz. Hard-wall boundary condition is used for the inner resonator surfaces, matched boundary condition is used for the side surfaces. Size of the scale bar is 48 mm. a) Pressure distribution in the simulation domain at the moment of focusing with the scatterer at the at the center (left) and the scatterer shifted (right) without resonators, b) Pressure distribution in the simulation domain at the moment of focusing with the scatterer at the at the center (left) and the scatterer shifted (right) with resonators, c) Normalized pressure recorded by the detector for the case of no resonators in the simulation domain, d) Normalized pressure recorded by the detector with resonators in the simulation domain

Chapter 4 Construction of the Ultrasonic Scanner

4.1. Components of the Experimental Setup

The experimental equipment used in the preliminary studies for the construction of the ultrasonic scanner consists of a function generator (Tektronix, AFG 3022B), spherical underwater transducers (ITC-1042), an underwater hydrophone, a dual-channel filter (Stanford Research Systems, Model SR650), an amplifier (Krohn-Hite, Model 7500), an oscilloscope (Agilent Technologies, DSO7104B), a translational stage (NewMark Systems, Model NLS4-12-16), a water-filled container and an array of Helmholtz resonators with a resonance frequency of 60.5 KHz as described in Chapter 3. The experiments were conducted on an aluminum optical table. Due to the expertise of our research group in underwater acoustics and previous underwater acoustic focusing experiments conducted by our group using Helmholtz resonators, the scanner is designed to work in water. Also, as explained earlier, water could be replaced by a different fluid that has impedance value close to that of finger. This would enable better coupling of acoustic waves to the finger ridges and help imaging deeper into the finger.

Once the amplifier amplifies the signals generated by the function generator, they are sent to the spherical underwater transducers. This causes vibration of the piezoelectric crystal inside the transducers and emanation of spherical waves. The acoustic signals travel through the transmitting medium – water and Helmholtz resonators inside it – and they are captured by the underwater hydrophone. The captured signals are further amplified and filtered by the dual-channel filter to increase the signal to noise ratio. Spacing between the underwater transducers and hydrophone is controlled by a translational stage, which is capable of moving in a plane parallel to the free water surface (Figure 13).

Each time the function generator sends a signal, it triggers the oscilloscope to record the measured data which is also stored in the computer memory. A Labview program controls the stage motion, oscilloscope and function generator settings, interactions between the components of the experimental system and acquisition of data.

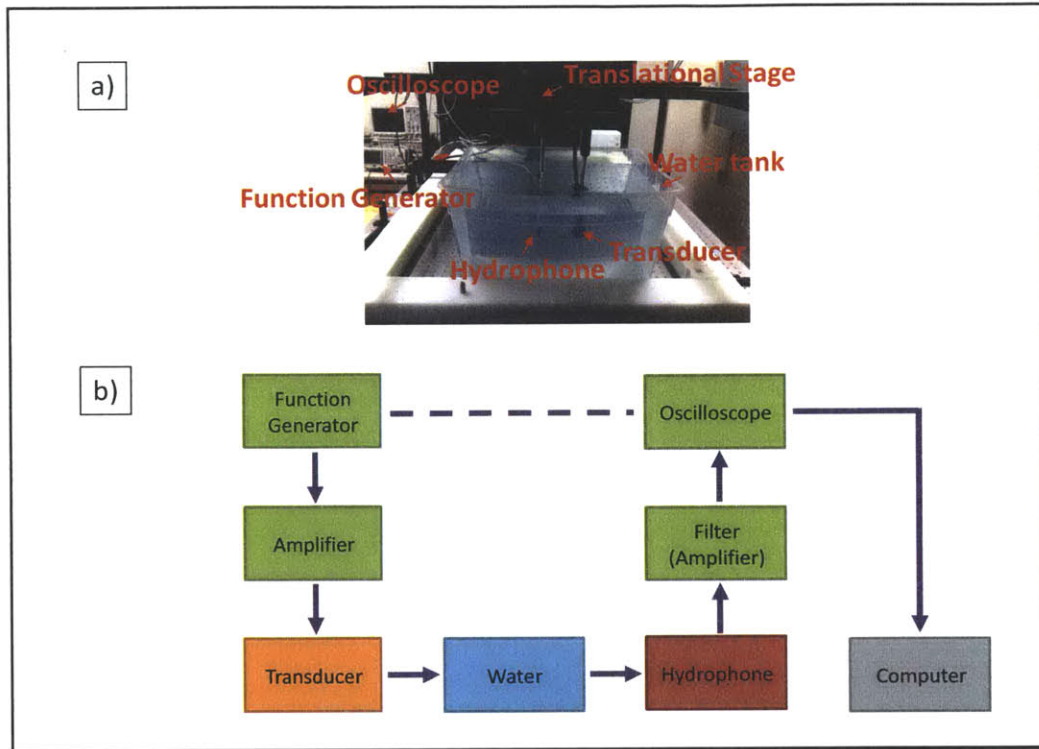


Figure 13 Components of the experimental setup. a) Photograph showing the experimental setup, b) Diagram showing the connections between the different experimental components.

4.2. Preliminary Experimental Results

Initial experiments are conducted using a single hydrophone and a single transducer without any Helmholtz resonators to better understand the acoustic signals sent and received. [35]

A shallow and wide water pool with a 5 mm thick glass base and polyethylene boundaries with a height of 10 cm is used as the water container (Figure 14-a). Ideally a wide water pool is expected to separate the reflection coming from the pool boundaries from the direct transmitted signals in time domain (which could affect the measured signal). Figure 14-b shows the waveform recorded by the underwater hydrophone, when sinusoidal waves with constant amplitude and a frequency of 60.5 KHz are sent from the spherical underwater transducer. The

recorded wave form does not exactly represent the constant amplitude sinusoidal waves sent from the transducer.

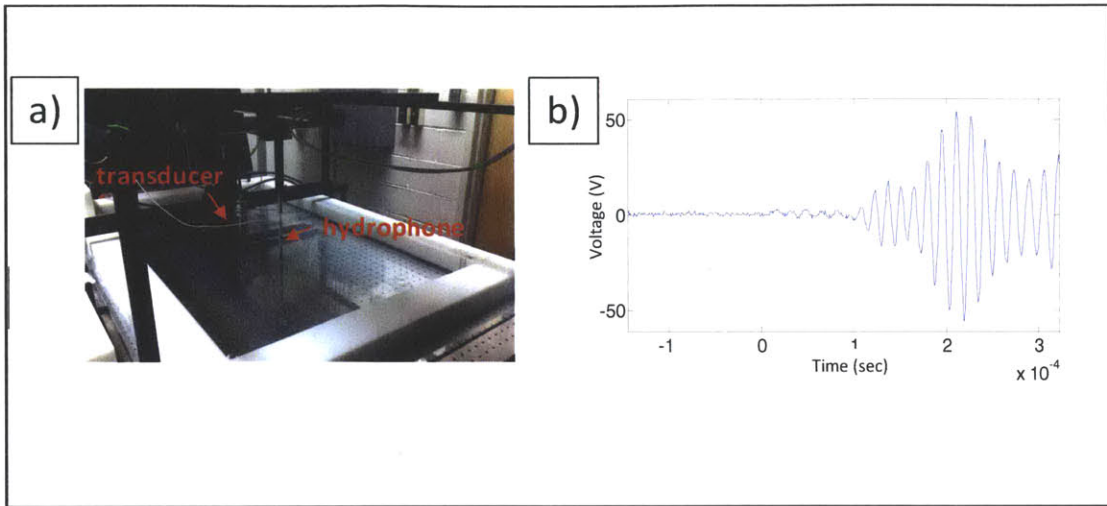


Figure 14 Experiments in the shallow water tank: a) Photograph of the experimental setup, b) Signal recorded by the hydrophone in a shallow water tank, when the transducer sends sinusoidal waves with frequency 60.5 KHz.

Simulations are done to better understand the propagation of the acoustic signals in the experimental system (Figure 15) and why the recorded signal looks as shown in Figure 14. The two dimensional simulation domain consists of layers of air, water, glass and aluminum representing the atmosphere, water in the shallow pool, glass base of the shallow pool and the optical table, respectively. Simulation results show that acoustic waves travelling in the water layer get coupled to the glass layer at the base of the water pool. Since speed of sound in glass (4500 m/s) is about three times as fast as the speed of sound in water (1482 m/s), waves travelling through the glass layer move ahead of the waves travelling through the water layer, can reach the hydrophone earlier and also leak back into the water layer (Figure 15). This leads to the complicated wave form first increasing and then decreasing in amplitude as shown in Figure 14-b. The acoustic source should be located sufficiently far away from the bottom surface of the water container to eliminate coupling of acoustic waves to the bottom surface of the tank. We then coated the bottom surface of the tank with a thin layer of rubber to eliminate wave coupling to the tank base, but this did not improve the results. A much thicker layer of rubber coating could be used for bottom coating and the height of the pool boundaries could be

increased, but this would complicate the current setup which was already leaking water from the pool boundaries.

As a simple solution, experiments with a single hydrophone and single transducer are repeated in a deeper plastic water tank (Figure 16-a, Figure 13-a). Different experiments are conducted to observe the influence of various parameters such as distance between transducer/hydrophone tip and free surface of water in the water tank, distance between transducer/hydrophone tip and bottom surface of the water tank, number of sine pulses sent, changes in waveform and frequency of the acoustic signal used, changes in type of acoustic source used.

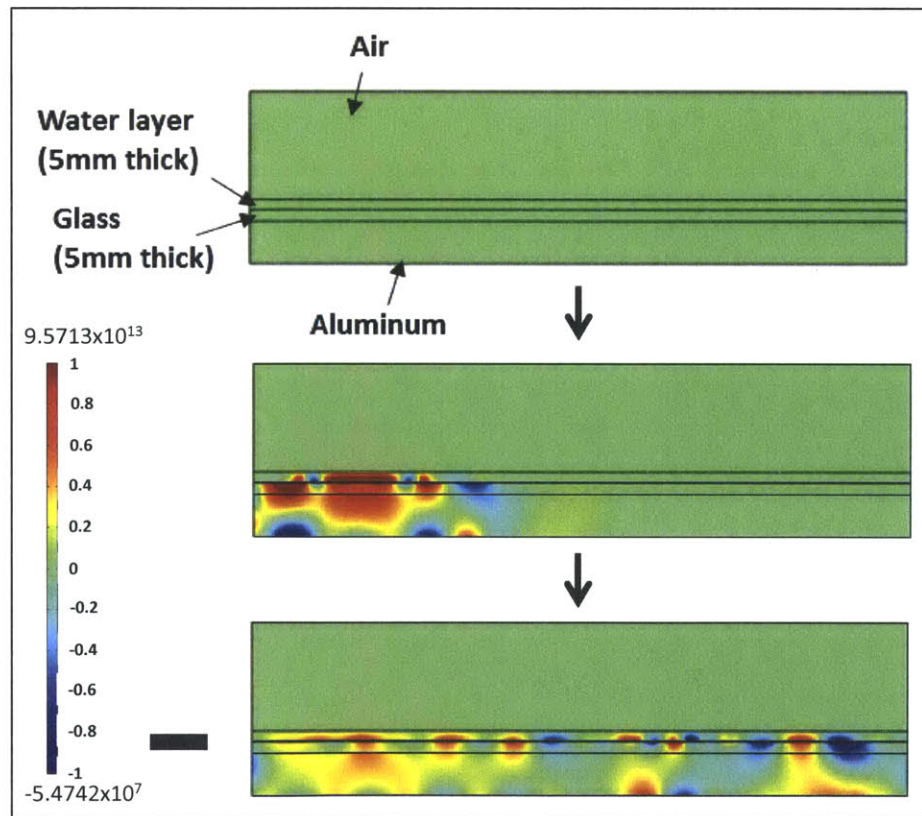


Figure 15 Simulation results showing the propagation of pressure waves through the experimental system, once an acoustic pulse is emitted in the 5 mm thick water layer. Arrow points in increasing time direction. Mediums of wave propagation are air, water, glass and aluminum from top to bottom. Frequency of the acoustic source is 60.5 KHz.

Hard-wall boundary condition is used for the outer boundaries. Size of the scale bar is 2 cm.

In order to separate reflections coming from boundaries of the water tank from the direct transmitted signal through the thin layered sample, and to prevent coupling of acoustic waves to the bottom of the container, we setup the experiments in a deep plastic water-filled container, with the dimensions shown in Figure 16-a. In this specific experimental configuration, the plastic tank is filled with water to a level of 24 cm. The tip of the transducer and the hydrophone is located 12 cm from both the free surface of water and bottom surface of the container. A sample signal recorded with the hydrophone is shown in Figure 16-b, where the parts of the signal corresponding to the reflections coming from different boundaries is identified. Recorded times for the arrival of different reflections (Figure 16-b) almost match with the calculated values given in Table 1.

Table 1 Distance the acoustic signals travel till reaching the hydrophone and expected time of arrival for the acoustic signal to reach the hydrophone, assuming speed of sound in water of 1482 m/s.

	Reflection Distance	Time
Bottom Wall	28 cm	189 μ sec
Transducer	45 cm	300 μ sec
Side Wall	48 cm	323 μ sec
Front Wall	51 cm	340 μ sec

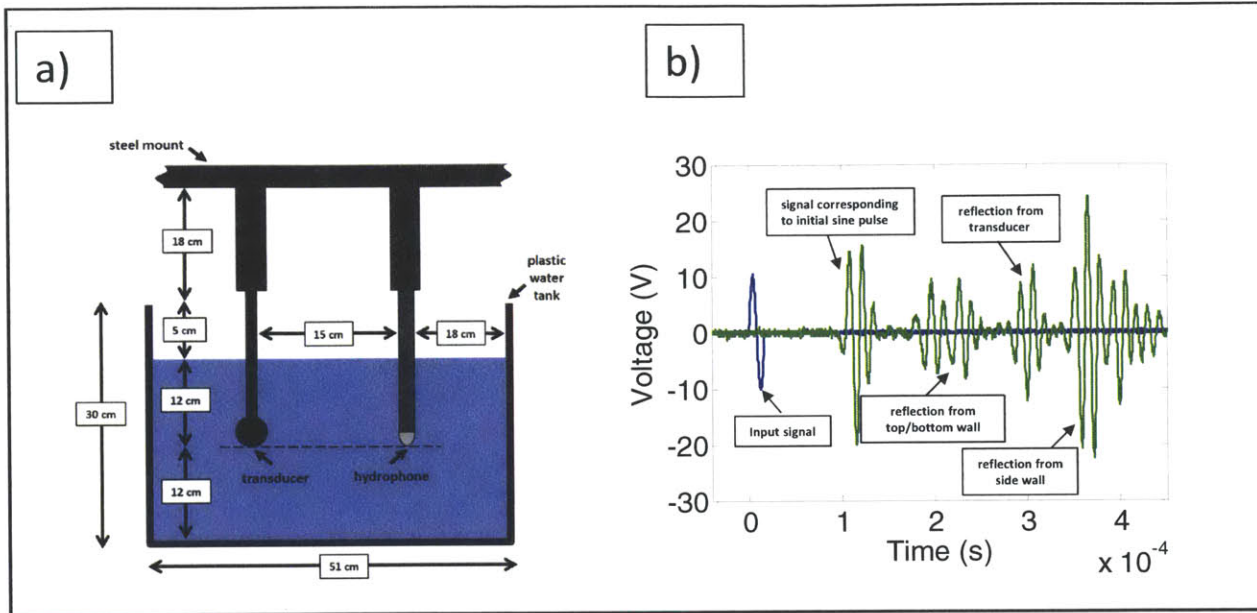


Figure 16 Experiments performed in the plastic water tank. a) Drawing of the experimental setup with dimensions, b) Sample acoustic signal measured with the hydrophone

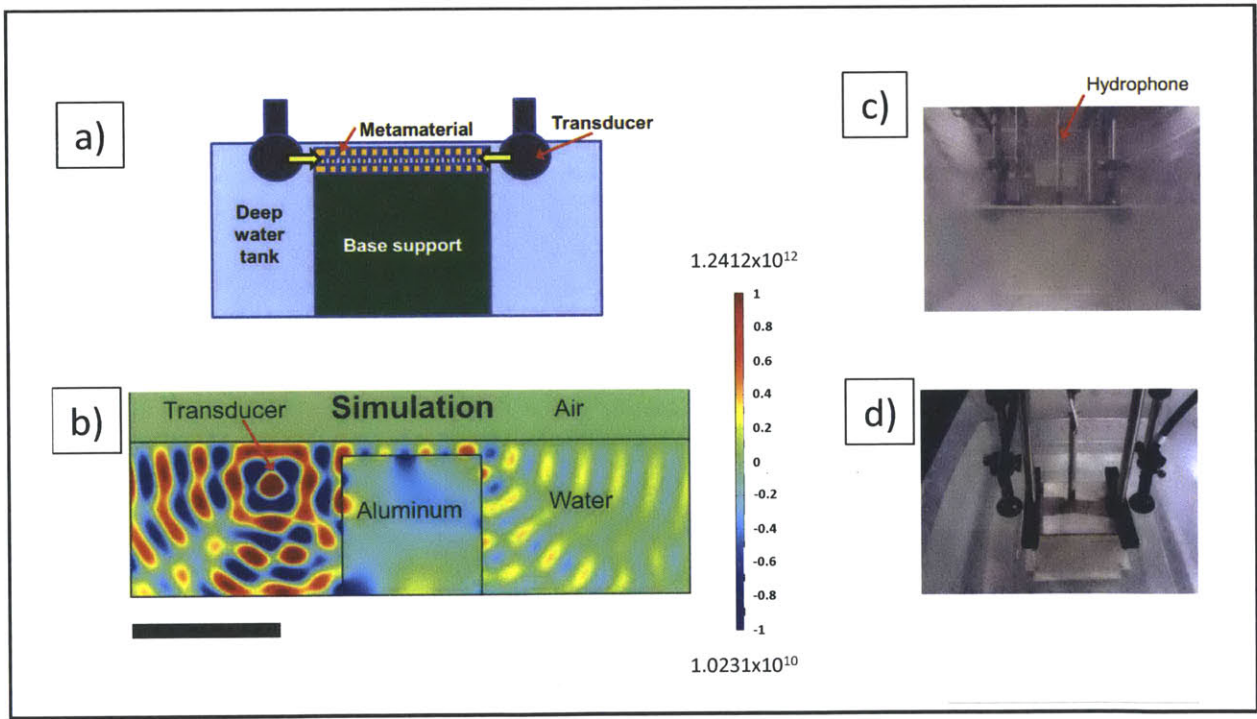


Figure 17 Prototype fingerprint imaging device. a) Drawing of the prototype fingerprint scanner, b) Simulations showing that a thin water layer can act as a waveguide. Mediums of wave propagation are air, water, and aluminum from top to bottom. Frequency of the

acoustic source is 60.5 KHz. Hard-wall boundary condition is used for the aluminum boundaries, matched boundary condition is used for the outer boundaries. Size of the scale bar is 12 cm c) Photograph showing the experimental setup from the side, d) Photograph showing the experimental setup from the top.

4.3. Prototype Ultrasonic Scanner

Based on the results obtained in the previous section, a new experimental system is designed to obtain acoustic focusing over an array of Helmholtz resonators and detect objects by measuring the scattered pressure field. Another goal of the experiments is to observe how the size of the focal spot obtained by interference of acoustic waves changes due to the presence of the Helmholtz resonator array. In the experiments, acoustic focusing is achieved using only two transducers.

Experimental results from the previous section indicate that the Helmholtz resonator array should be placed 12 cm away from the bottom surface of the water tank to track the location of the initial wave front as the acoustic waves move inside the Helmholtz resonator array. Therefore, a stainless steel block of dimensions 12cm x 12cm x 12cm, on which the Helmholtz resonator array is placed, is fabricated. The sample is then integrated into the new experimental setup (Figure 17, 18-a).

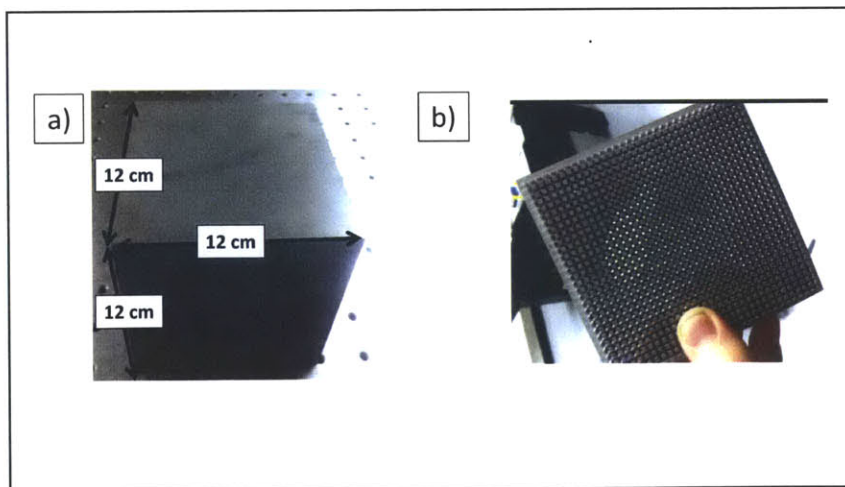


Figure 18 Photographs of: a) Stainless steel block with dimensions 12 cm x 12 cm x 12 cm, b) Helmholtz resonator array placed on top of the resonator array.

Initially, a hollow rectangular cavity with walls made by 3D-printed plastic, is placed on top of the resonator array that rests on the metal block (Figure 17). The rectangular cavity is designed to enable coupling of acoustic waves into the Helmholtz resonator array: it keeps the sides of the Helmholtz resonators open for acoustic signal transmission into the resonators and blocks acoustic wave motion over the resonators. The height of the plastic rectangular cavity is 11 cm and it contains three different layers of plastic material: inner layer 3.175 mm in thickness, middle layer 8.825 mm in thickness and containing air gaps and outer layer 4.725 mm in thickness. The aim in using different rubber material and integrating air gaps is to create a soundproofing material. The hydrophone is placed inside the hollow rectangular cavity, so that it can move over the resonator surface to measure the pressure field. However, experiments done with the rubber setup show that acoustic waves could still be transmitted through the thick rubber walls of the hollow rectangular cavity and it is not possible to fully couple acoustic waves into the Helmholtz resonators. Stainless steel layers, 1 mm in thickness, are placed on the inner and outer surfaces of the hollow rectangular cavity to improve the design, but the system still could not effectively block acoustic waves. Therefore, the experimental setup is modified to enable better coupling of acoustic waves to the resonator array.

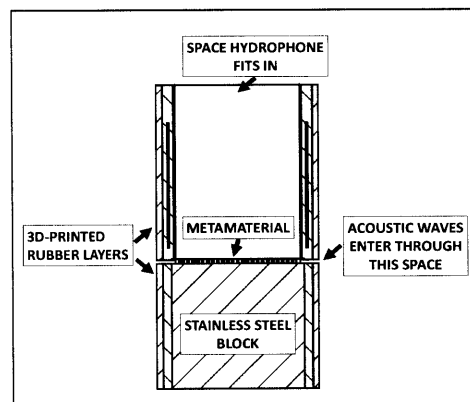


Figure 19 Cross sectional view of the 3D-printed rubber setup for coupling acoustic waves to Helmholtz resonators

In the new experimental configuration, the plastic tank is filled with water such that only a thin layer (less than one wavelength in thickness) of water remains on top of the stainless steel block (Figure 17-b). This thin water layer is shown to act as a waveguide (a structure which can guide and carry waves) as shown by the simulations performed (Figure 17-b), when transducers

send acoustic waves towards the thin water layer. When the Helmholtz resonator array is placed inside this thin water layer, acoustic waves coming from the sides are expected to be coupled into the Helmholtz resonator array.

It is our expectation that this experimental setup would form the most basic system to investigate how the focal spot size changes due to different metamaterial geometry during acoustic focusing and to acoustically detect objects placed over the Helmholtz resonators. Experiments are performed to compare the size of the interference region obtained using two transducers with and without resonators as described below.

4.4. Experimental Results and Discussion

Figure 23 and Figure 24 show experimentally obtained snapshots when two spherical acoustic sources are placed near the samples [37]. The videos are obtained by scanning the pressure field over the stainless steel block with a hydrophone as 5 cycles of sine waves (with frequency 60.5 KHz) are sent from the transducers. Further details of the experimental configuration are given in the Appendix. Figure 23 shows experimental results obtained with the underwater hydrophone, when the aluminum block is only covered by a thin water layer during the scanning process. In comparison, Figure 24 presents the results obtained when the Helmholtz resonator array is also present in the thin water layer as scanning with the hydrophone proceeds. Spacing between the hydrophone scanning points is equal to 3.75 mm, which is the spacing between the holes in the Helmholtz resonators. Additional experiments are also done with a metal plate which contains an array of through holes that are separated by 3.75 mm apart. The plate is lifted to the same height as the Helmholtz resonator array by placing small metal blocks on its four corners. In comparison to the Helmholtz resonator array, the plate enables easier access of acoustic waves to the hydrophone scanning locations. Plots of the time domain signals obtained from experiments involving water, holey plate and Helmholtz resonators are shown in Figure 21.

Figure 20 shows the simplified schematic of a two point source interference pattern which we expect to observe in the experiments. In the schematic nodal points formed by the constructive interference of the wave forms coming from the two acoustic sources, and anti-

nodal points formed by the destructive interference of wave forms coming from the two acoustic sources are indicated by red and blue dots. The pressure pattern formed is a standing wave pattern, which is characterized by the presence of nodes and antinodes that are always located at the same positions. The antinodes lie on anti-nodal lines and the nodes lie on nodal lines. The interference pattern is characterized by an alternating pattern of nodal and anti-nodal lines.

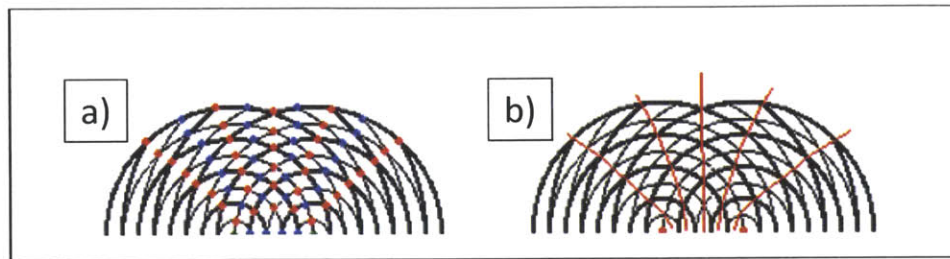


Figure 20 Schematic showing the two point source interference pattern. Wave crests are shown by thick lines and wave troughs are shown by thin lines. a) Demonstration of two sources (green), nodal points (blue), anti-nodal points (red). b) Demonstration of anti-nodal lines (red). Figure is adapted from reference [37].

Below is a summary of experimental results and observations obtained from the experiments:

- 1) Experimental results show that the acoustic waves coming from the two acoustic sources form the expected interference pattern at the center of the metal block when no resonators are present in the experimental system (Figures 23 and 25, blue solid circles). Anti-nodal and nodal points can be clearly identified in the experimental results without Helmholtz resonators. The center region in between the two sources where the waves always meet constructively attains a minimum width of about half the wavelength (around 12 mm), due to the diffraction limit. We also term this center region as focal spot in the thesis.
- 2) As an intermediate step, when the plate with holes is placed over the metal block, a clear focal spot could be observed. The measured pressure amplitude is slightly lower, but the width of the observed interference region is still close to half -wavelength (Figure 25, Green solid circles).

- 3) When the array of Helmholtz resonators are placed over the metal block, the measured acoustic signals are weaker, and a clear interference region could not be observed. Therefore, a comparison of the size of the interference region with and without resonators, to show that the resonators lead to a reduction in the focal spot size, could not be made. Even when working with continuous sinusoidal waves and after waiting for minutes so the system reaches steady state, no significant change in the results is observed. Furthermore, amplitude of the recorded pressure field was observed to be significantly lower compared to the experiments done without Helmholtz resonators.

Below is a discussion and comparison of the results obtained:

- 1) Both the experiments and the simulations (from Chapter 3) show that during acoustic focusing without Helmholtz resonators diffraction limits the size of a focal spot obtained. Even though simulations verify that the diffraction limit can be beaten using Helmholtz resonators, the same result could not be shown experimentally.
- 2) Both the holey plate and the Helmholtz resonator array can be considered as metamaterials. Both types of metamaterials form effective media in which the speed of acoustic waves is slower (due to the metamaterial geometry interfering with acoustic wave motion). Since the speed of sound is reduced in the metamaterial, the effective wavelength should also be reduced for a fixed frequency value. Therefore, the shorter effective wavelength would be expected to result in a smaller focal spot during acoustic focusing experiments.
- 3) In the experiments involving the holey plate, a clear focal spot could be obtained due to the fully open space below the holey plate, allowing easy access of acoustic waves to the system. That there is no reduction in the size of the focal spot obtained with the holey plate indicates that the plate with holes is not very effective in reducing the speed of waves moving under it.

4) By making a comparison of the time domain signals (Figure 21), the following can be concluded: 1) Highest decay in pressure is observed for the experiments involving the Helmholtz resonators, 2) Lowest decay in pressure is observed for the experiments done in the thin layer of water, 3) The recorded wave forms do not coincide with each other, suggesting that the acoustic signals move at different speeds through each medium. Phase delay between the acoustic signals moving through the thin water layer and the holey plate is insignificant. However, the acoustic signals moving through the metamaterial experience a significant phase delay.

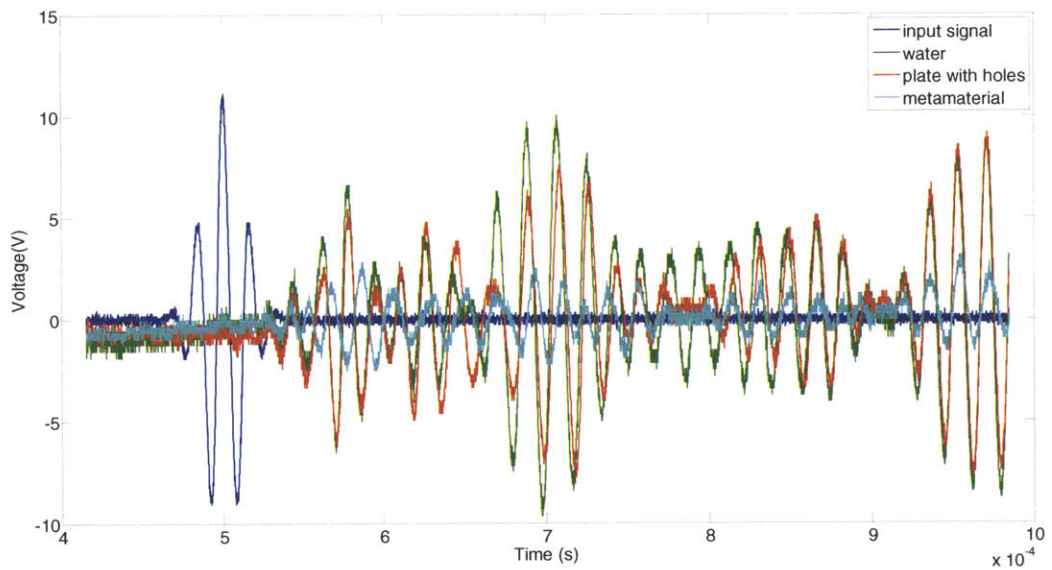


Figure 21 Time domain signals measured for at the same hydrophone position for three different experimental configurations.

Additional simulations are done to better understand the experimental results with two transducers for two different cases: 1) with Helmholtz resonators, 2) without Helmholtz resonators. The simulation domain is the same as in the case of simulations of Section 3, but the only differences are: 1) two point sources are used in the simulations, 2) point sources are placed at the center points of the edges of the resonators, 3) point sources send 5 continuous sine waves. A description of the simulation domain with Helmholtz resonators is shown in Figure 22-a for clearness.

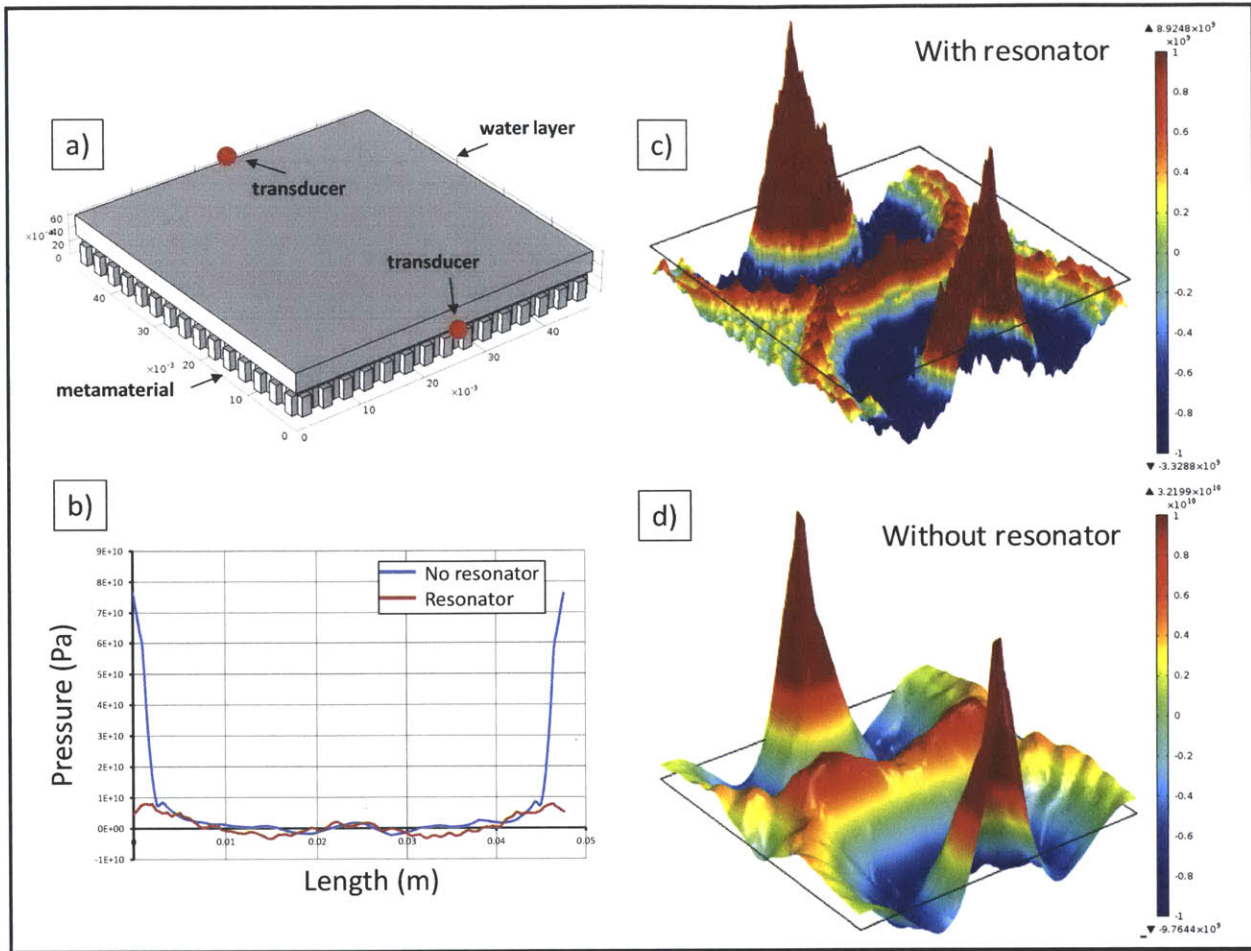


Figure 22 COMSOL simulations for acoustic focusing using two transducers: a) The simulation domain: Hard-wall boundary conditions are used for the inner resonator surfaces, matched boundary conditions are used for all the other (side) surfaces. Dimensions given on the figure have units of meters, b) Pressure distribution along a line joining the two acoustic sources with and without resonators, c) 3D representation of the pressure distribution in the simulation domain with resonators when the central interference region has minimum width at $t = 1.98347$ sec, d) 3D representation of the pressure distribution in the simulation domain without resonators when central interference region has minimum width at $t = 1.98347$ sec. The medium of wave propagation is water. The acoustic sources send five continuous sine waves with a frequency of 60.5 KHz. Each edge of the simulation domain is 47.6 mm in length.

Results obtained in COMSOL for cases with and without resonators are shown in the Figures 26 and 27. Simulation results without resonators (Figure 26) match with the experimental results (Figure 23) completely. Simulation results with the Helmholtz resonators (Figure 27) demonstrate the interference pattern that would be observed, if the experimental setup worked perfectly.

Figures 28 and 29 show simulation results describing how wave fronts propagate through the systems with and without Helmholtz resonators. A delay in the waves moving through the medium with Helmholtz resonators is clearly observed, which shows that the waves have lower effective speed in the Helmholtz resonator array. Size of the high pressure region in the middle is also observed to be smaller with Helmholtz resonators in the simulation domain. Rough calculations show that speed of sound in the Helmholtz resonator array is about 1370 m/sec (which is less than the speed of sound in water) and size of the interference region in the presence of resonators is about 9.5 mm which is sub-wavelength (Figure 22 b-c-d). These simulation results confirm our discussions above that: 1) effective sound speed is smaller in the Helmholtz resonator array, 2) the Helmholtz resonators would cause the conversion of evanescent waves to propagating ones so a sub-wavelength focal spot would be observed, if the experimental setup worked properly.

The differences in results obtained in the experiments and simulations are due to the following:

- 1) In the simulations, there is an infinite water layer on top of the resonators, but in the experiments there is a thin water layer and air on top of the resonators.
- 2) In the simulations, waves are emanated from a source located inside the resonators, but in the experiments waves are emanated from a source outside the resonators.
- 3) In the experiments, the waves move through two different layers: a) the thin water layer on top of the resonators, b) the region inside the resonators. Interactions between these two layers may be affecting the results badly.
- 4) Use of sound hard boundaries for the resonators instead of using acoustic structure interaction simplifies the simulations.

5) In the simulations, there are no reflections coming from the outer boundaries of the system due to the impedance matched outer boundaries used. In the experiments, acoustic waves which cannot enter the resonator domain through the inlet section at the front, move towards the sides of the resonator array and enter the resonators from the side openings. The confined spaces between the side faces of the plastic tank and side surfaces of the Helmholtz resonator array act as passages which direct acoustic waves into the resonators. Furthermore, acoustic waves reflected from the boundaries of the plastic tank affect the experimental results, since the plastic water tank has a finite size.

Improvements need to be done to the current experimental setup to enable better coupling of acoustic waves into the Helmholtz resonator array. One solution would be to use focused beam transducers and higher amplification values to obtain a more clear interference pattern. Furthermore, a metal sheet with very high impedance could be placed at the section of the Helmholtz resonators where the acoustic waves enter into the resonators. The metal plate could leave only the inlet section of the resonators open and cover the surrounding region to block acoustic waves (and prevent reflections). Another solution would be to revisit the experimental setup, which contains the hollow rectangular cavity with rubber walls. As discussed previously, the experimental setup with the hollow rectangular cavity is not effective in blocking acoustic waves travelling over the resonator array. Therefore, acoustic waves coming from the transducers cannot be fully coupled into the resonators. If this experimental system can be redesigned with thicker steel walls, then propagation of acoustic waves over the resonator array can be prevented. By the use of focused beam transducers, entrance of acoustic waves from the side openings of the Helmholtz resonator array can be prevented without leading to the formation of any reflected waves in the scanning area.

A reduction in the size of the interference region to a value below the half the wavelength limit would be expected to be observed in a successfully working experimental setup containing Helmholtz resonators. It would be a real challenge to miniaturize this system to form a real acoustic fingerprint sensor, as it would be more difficult to couple acoustic waves and prevent reflections in smaller scales.

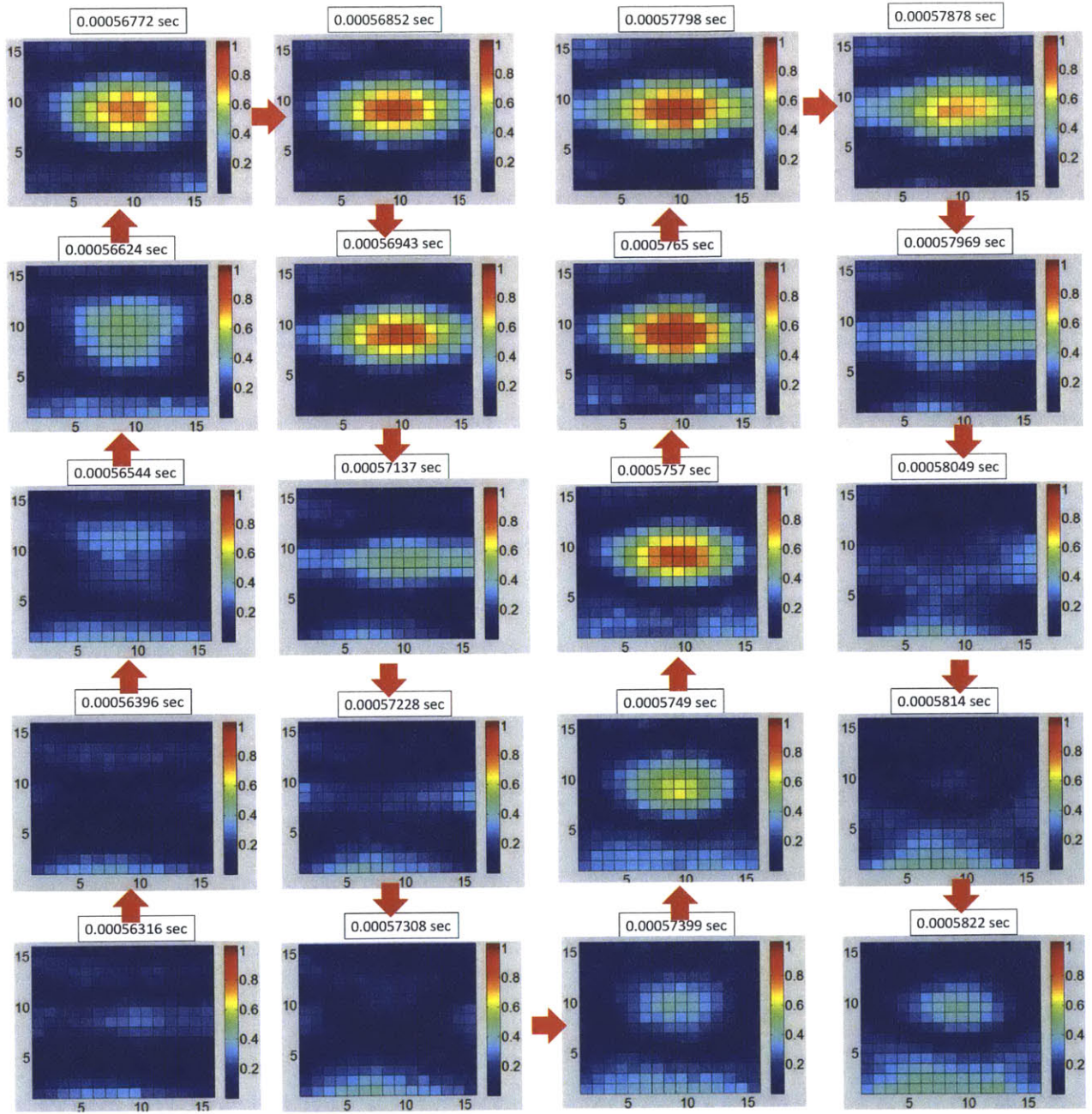


Figure 23 Interference pattern recorded over the surface of the stainless steel block without Helmholtz resonators placed on it. Arrows point in increasing time direction. Medium is water, frequency of acoustic source is 60.5 KHz, scale bar is 12 mm, time of capture for each snapshot is indicated above it. For snapshots 3 – 8, $(\text{frequency}) \cdot (\Delta t) \approx (1\text{E}-6)(60.5\text{E}3)=0.06$.

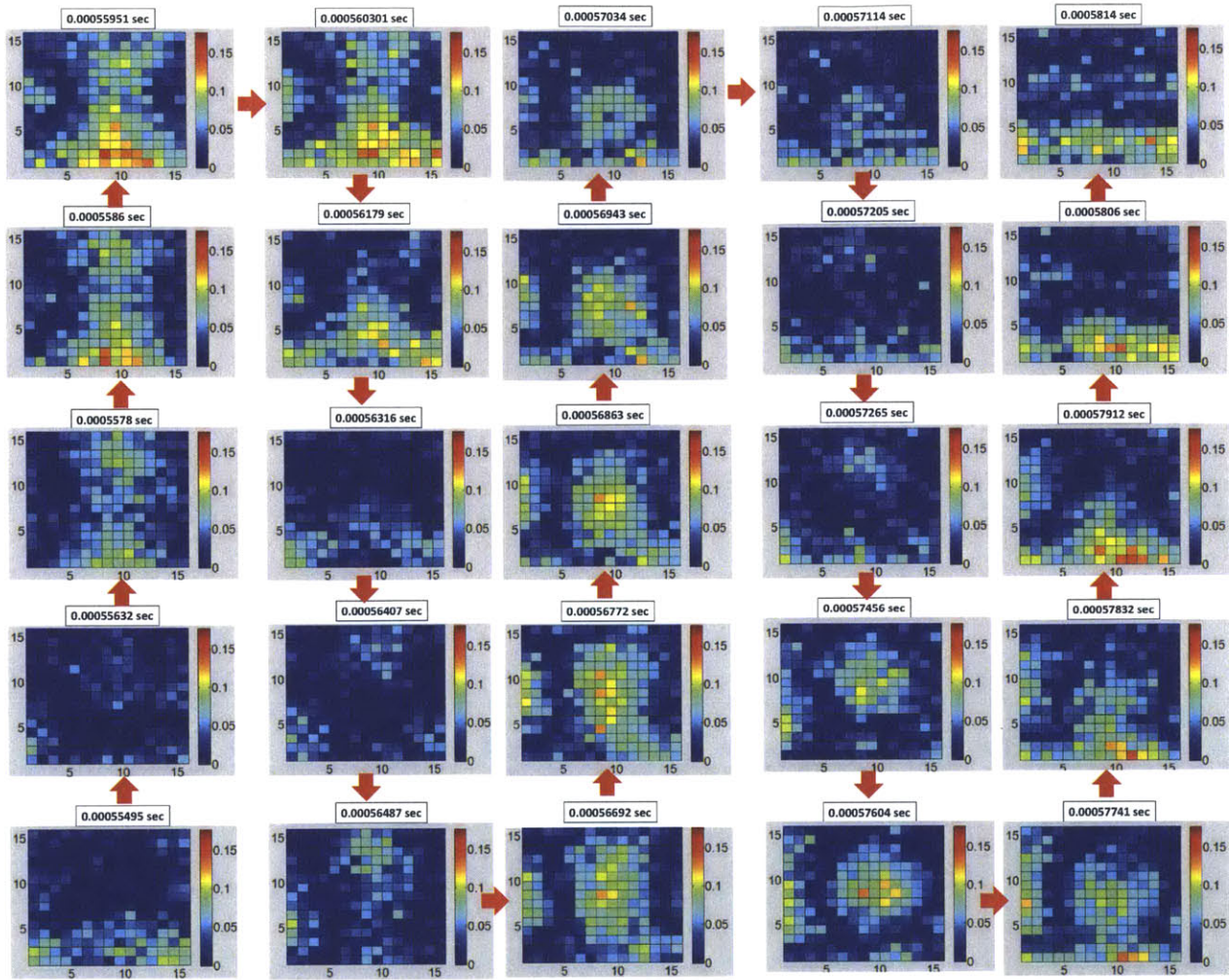


Figure 24 Interference pattern recorded over the surface of the stainless steel block with Helmholtz resonators placed on it. Arrows point in increasing time direction. Medium is water, frequency of acoustic source is 60.5 KHz, scale bar is 12 mm, time of capture for each snapshot is indicated above it. For snapshots 2-7, $(\text{frequency}) \cdot (\Delta t) \approx (1E-6)(60.5E3)=0.06$.

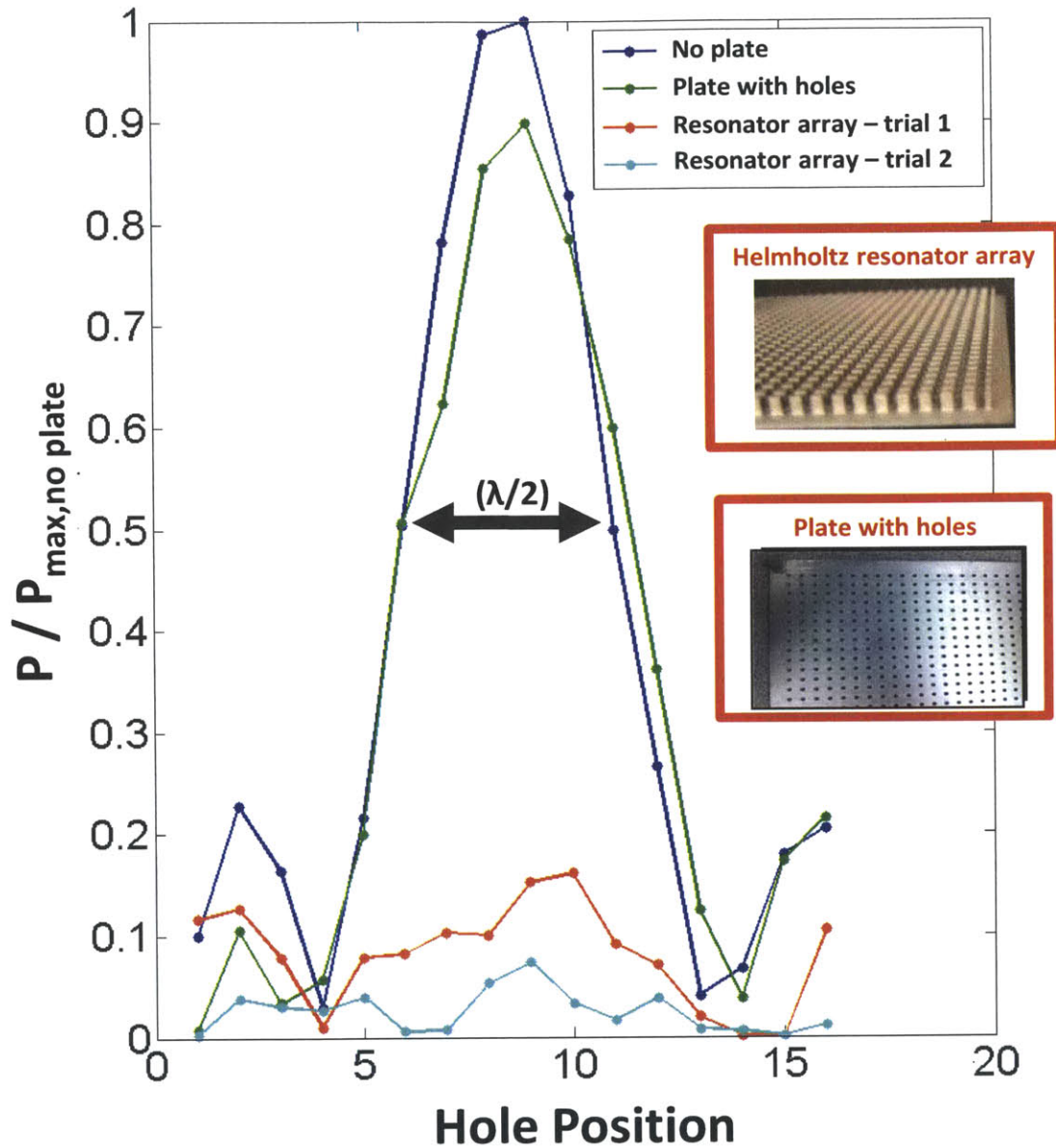


Figure 25 Variation of pressure along the line connecting two spherical transducers over the metal block surface for different experimental configurations: no plate on the metal block, plate with holes on the metal block, resonator array on the metal block. One unit corresponds to 3.75 mm which is the spacing between the holes. All the pressure values are normalized by the maximum pressure value measured for the case of no plate on the metal block.

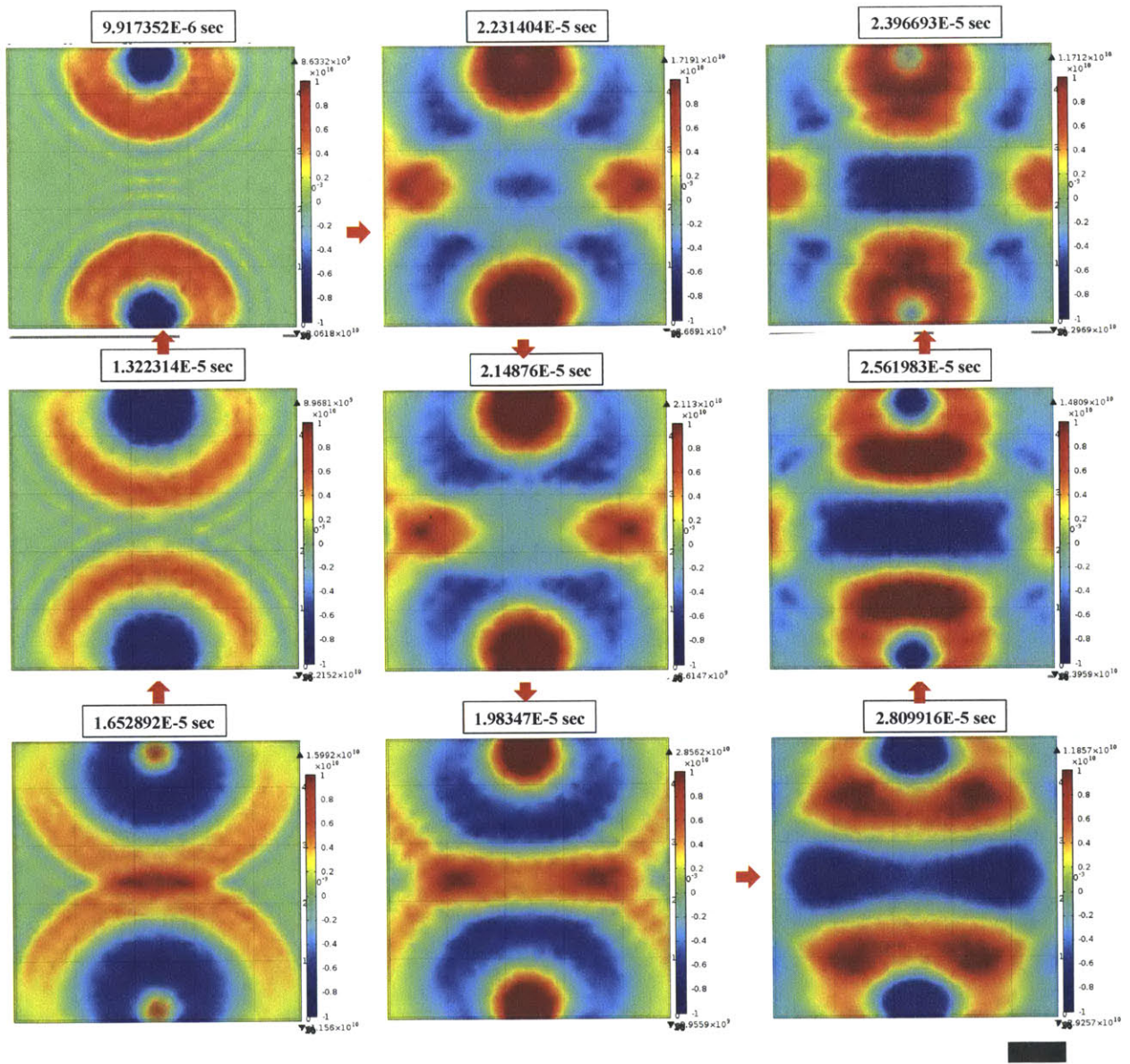


Figure 26 Two point source interference pattern obtained using COMSOL without any Helmholtz resonators in the simulation domain. Medium is water, frequency of acoustic source is 60.5 KHz, size of the scale bar is 10 mm, time of capture for each snap shot is indicated above it.

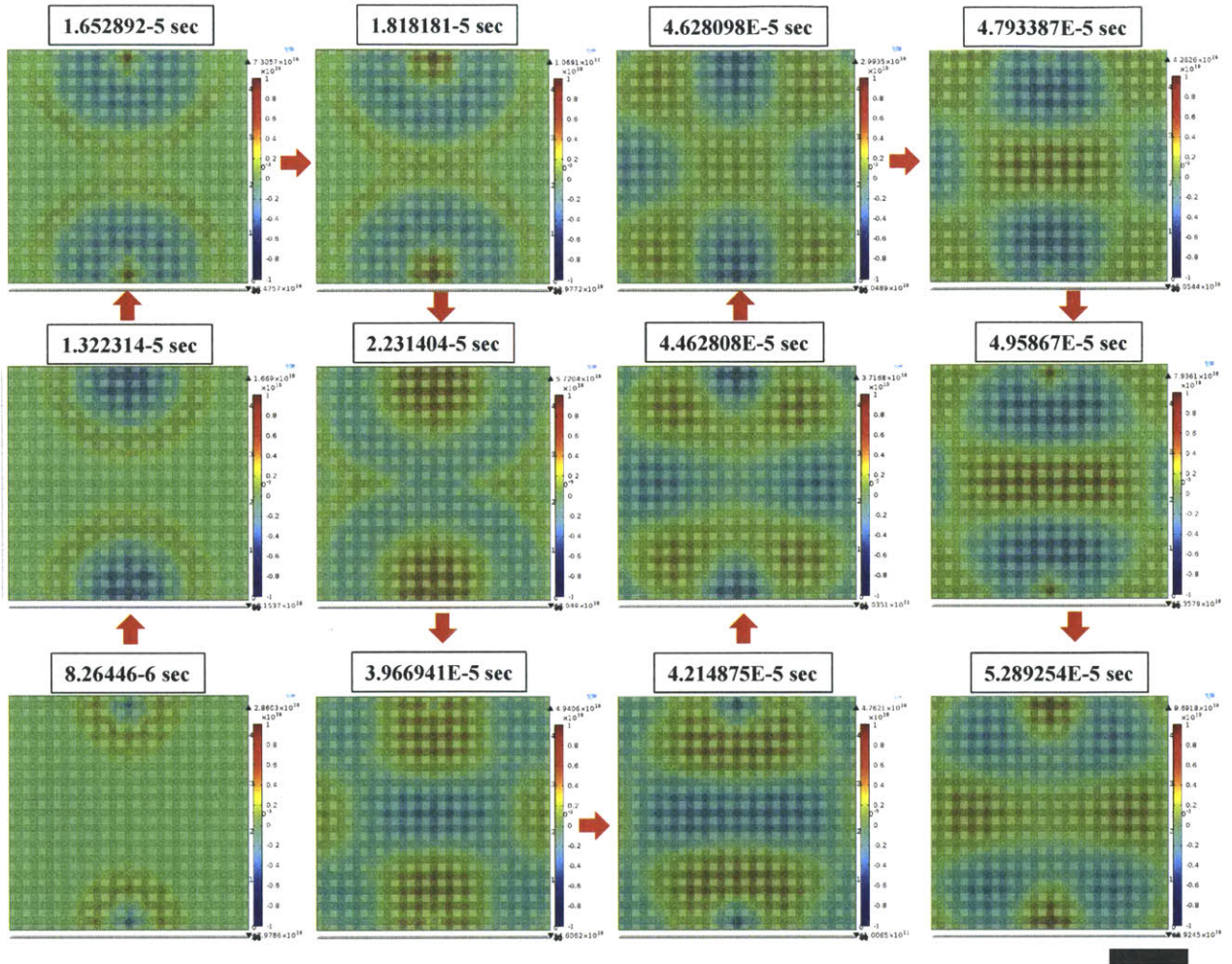


Figure 27 Two point source interference pattern obtained using COMSOL in the presence of Helmholtz resonators in the simulation domain. Medium is water, frequency of acoustic source is 60.5 KHz, size of the scale bar is 10 mm, time of capture for each snap shot is indicated above it.

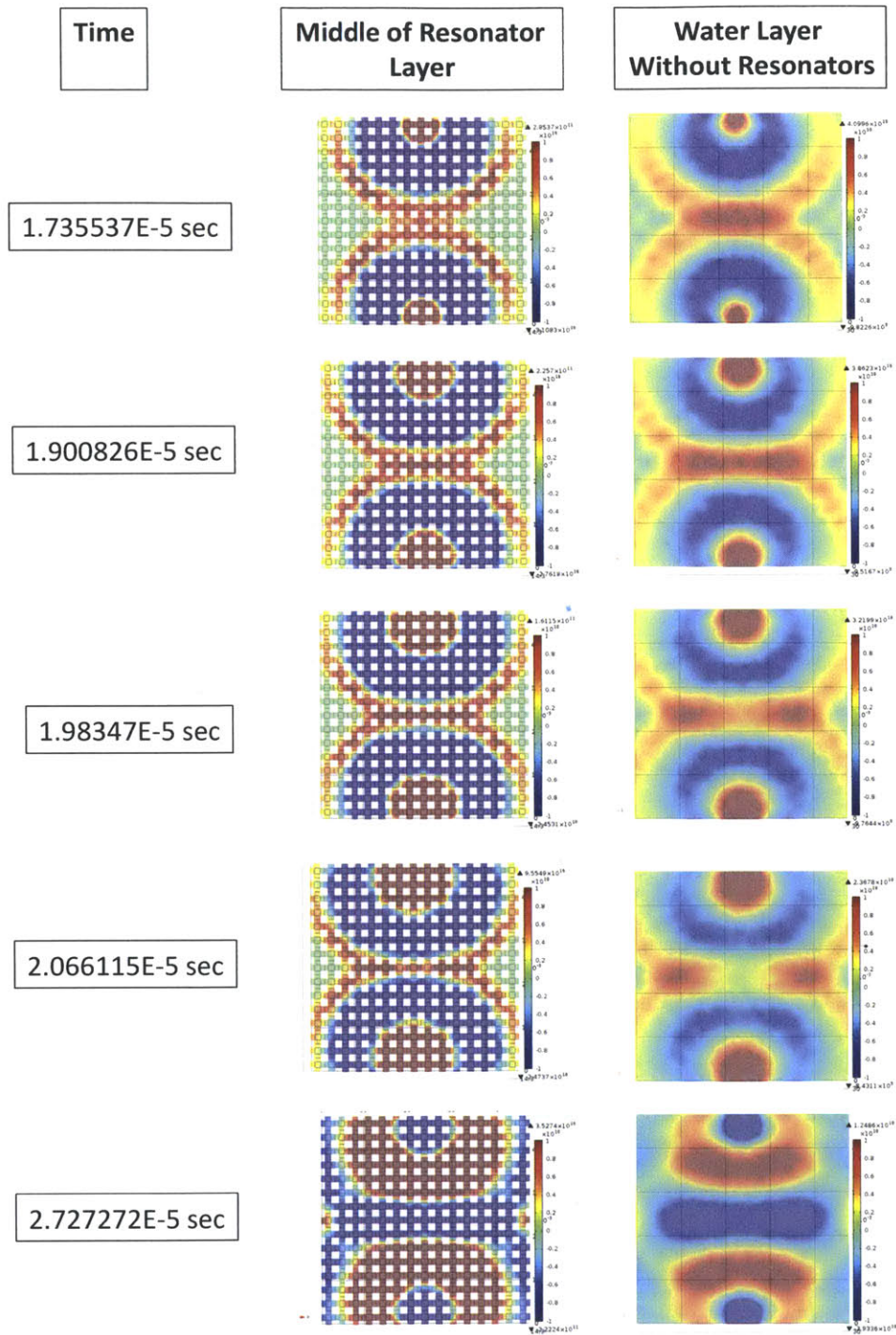


Figure 28 Snapshots showing the size of the constructive interference region at the center of the simulation domain with and without Helmholtz resonators at the same time steps. Medium is water, frequency of acoustic source is 60.5 KHz, each edge of the simulation domain is 47.6 mm in length.

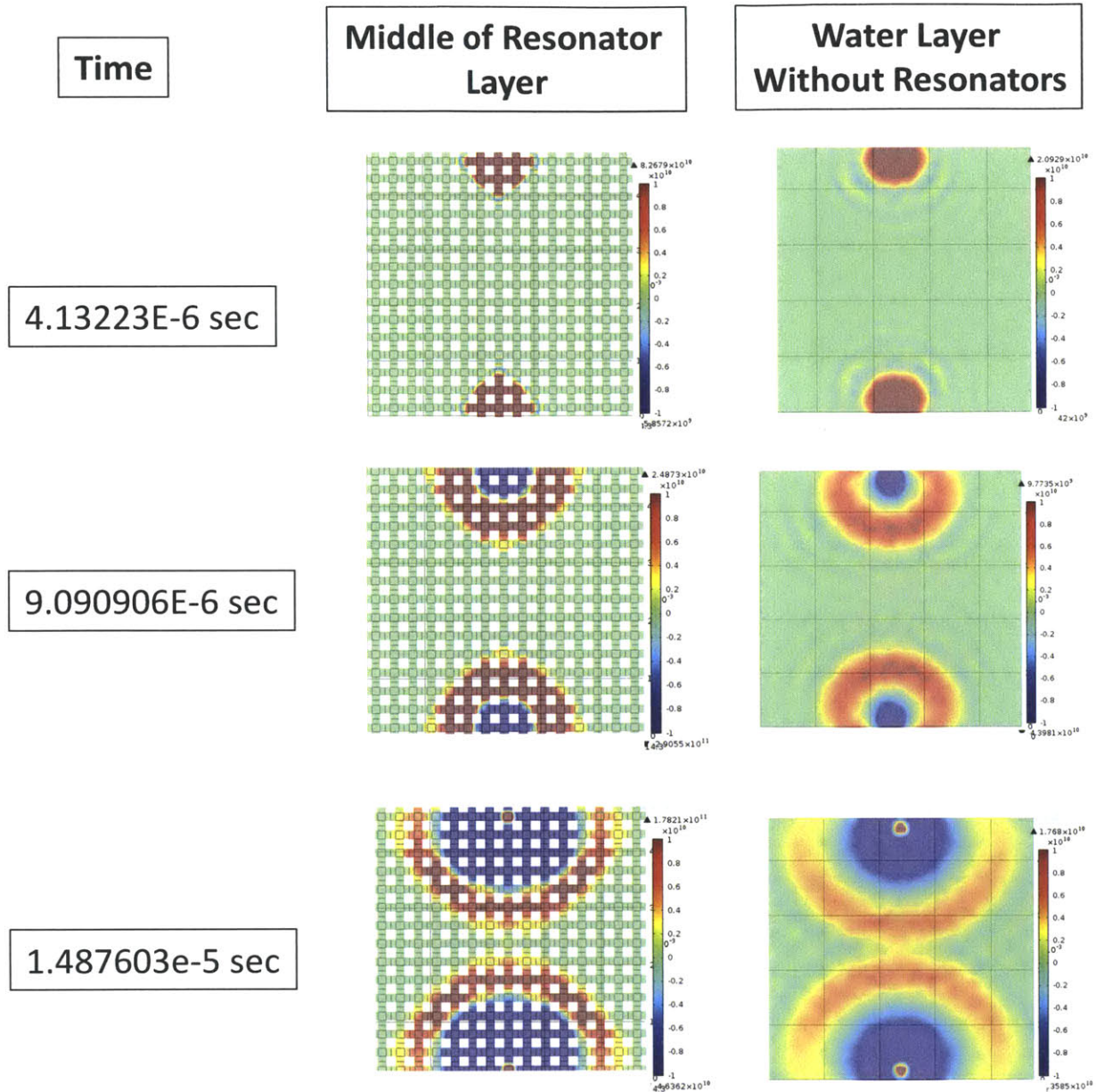


Figure 29 Snapshots showing the propagation of acoustic signals through simulation domains with and without resonators. Medium is water, frequency of acoustic source is 60.5 KHz, each edge of the simulation domain is 47.6 mm in length.

Chapter 5 Summary and Future Work

In this thesis, the design and construction of an ultrasonic fingerprint scanner which uses metamaterials is initiated. Simulations are performed to understand how acoustic signals propagate through the metamaterial layer, which show that sub-wavelength acoustic focusing could be achieved over an array of Helmholtz resonators. Tools are developed to better understand the propagation of acoustic signals and quantify information losses. These tools show great potential in the design of optimized metamaterial geometry for advanced ultrasonic fingerprint scanners. Experiments are performed to couple acoustic waves to an array of Helmholtz resonators and to demonstrate sub-wavelength acoustic focusing experimentally over the Helmholtz resonator array. Experiments are not successful despite trials with various experimental configurations.

The future work for the project described in this thesis would involve:

1) Improvement of the experimental system to enable better coupling of acoustic waves to Helmholtz resonators

- Use of focused beam transducers and higher amplification values to prevent acoustic waves coming into the resonator array from the openings on the side walls

- Placement of the resonator array into a metal casing with a funnel-like opening to better direct acoustic waves into the resonator array.

2) Better understanding acoustic signal transmission through resonant structures

- Focal spots sizes and acoustic signal speeds for resonator arrays with different geometries could be compared through experiments and simulations to have a better understanding of acoustic signal transmission through different resonant structures.

- The cavity under the plate with holes could be filled with air bubbles, and the characteristics of air bubbles could be identified by comparing properties of signals being transmitted through this medium.

3) Conversion of the system into an actual acoustic imaging device and experimental verification that the system can be used for detection of smaller objects placed over the resonators.

4) Addition of thermocouples to the experimental system and investigating its performance as an acoustic heating system.

5) Down-scaling of the experimental setup to couple acoustic waves to an array of miniaturized Helmholtz resonators at MHz frequencies.

6) During the processes of designing the fingerprint scanner, studies on measuring acoustic signal transmission through air bubbles with silica shells are also conducted which are not presented in this thesis. The analysis done with the Helmholtz resonators could be applied to these air bubbles for the purpose of using air bubbles in an imaging device as a lens.

7) Placement of resonating structures in the simulation domain used to obtain the propagation operator and determination of the resonator geometry that leads to singular values with the highest magnitude.

References

- [1] J. K. Scheneider, “Ultrasonic Fingerprint Sensors”, Advances in Biometrics: Sensors, Algorithms and Systems, edited by N. K. Ratha and V. Govindaraju, Springer, London 2008.
- [2] Y. Saijo *et al.*, “High Frequency Ultrasound Imaging of Surface and Subsurface Structures of Fingerprints”, Proceedings of the 30th Annual International IEEE EMBS Conference, 2008.
- [3] R. Gr. Maev *et al.*, “High Resolution Ultrasonic Method for 3D Fingerprint Representation in Biometrics”, Acoustical Imaging, I.Akiyama Editor, Springer, Japan, 2008.
- [4] J. K. Schneider *et al.*, “Live scan fingerprint imagery using high resolution C-scan ultrasonography”, Proceedings. 25th Annual 1991 IEEE International Carnahan Conference on Security Technology, 1991.
- [5] J. K. Scheneider *et al.*, “Ultrasonic Imaging Systems for Personal Identification”, www.ultra-scan.com.
- [6] W. S. Gan, “Acoustical Imaging: Techniques and Applications for Engineers”, Wiley, United Kingdom, 2012.
- [7] J. M. Sanches *et al.*, “Ultrasound Imaging: Advances and Applications”, Springer, United Kingdom, 2012.
- [8] T. L. Szabo *et al.*, “Diagnostic Ultrasound Imaging: Inside Out (Biomedical Engineering)”, Elsevier, United Kingdom, 2004.
- [9] J. Ashbourn, “Advanced Identity Verification: The Complete Guide”, Springer, United Kingdom , 2000.

- [10] N. Samir, M. Thieme, and R. Nanavati, "Biometrics: Identity Verification in a Networked World", Wiley and Sons, New York, 2002.
- [11] N. Grew, "The Description and Use of the Pores in the Skin of the Hands and Feet", Philosophical Transactions of the Royal Society of London, 14, 1684.
- [12] M. Malpighi, "Anatomical Observations of the External Organs of Touch", Aegidius Longus, Italy, 1685.
- [13] R. L. Donald, "Dr. Henry Faulds - Beith Commemorative Society", Journal of Forensic Identification, 53, 2003.
- [14] F. Galton, "Finger Prints", MacMillan and Co., London, 1892.
- [15] R. K. Tewari and K. V. Ravikumar, "History and Development of Forensic Science in India". Journal of Postgraduate Medicine, 46, 2000.
- [16] N. Ratha and R. Bolle, "Automatic Fingerprint Recognition Systems", Springer, New York, 2004.
- [17] D. Maltoni, D. Maio, A. K. Jain and S. Prabhakar , "Handbook of Fingerprint Recognition", Springer, United Kingdom, 2009.
- [18] S. A. Cole, "Suspect Identities: A History of Fingerprinting and Criminal Identification", First Harvard University Press, United States, 2001.
- [19] www.ultra-scan.com
- [20] E. Hecht, "Optics", Pearson Education, United States, 2008.
- [21] J. Zhu *et al.*, "A Holey-structured Metamaterial for Acoustic Deep -Subwavelength Imaging", Nature Physics, 7, 2011.
- [22] F. Lemault *et al.*, "Acoustic Resonators for Far-Field Control of Sound", Physical Review Letters, 107, 2011.

- [23] S. Zhang *et al.*, “Focusing Ultrasound with an Acoustic Metamaterial Network”, *Physical Review Letters*, 102, 2009.
- [24] N. Fang *et al.*, “Ultrasonic Metamaterials with Negative Modulus”, *Nature Materials*, 5, 2006.
- [25] R. V. Craster and S. Geunneau, “Acoustic Metamaterials: Negative Refraction, Imaging, Lensing, Cloaking”, Springer, United Kingdom, 2012.
- [26] G. Strang, “Linear Algebra and Its Applications”, Harcourt Brace Jovanovich, United States, 1988.
- [27] H. C. Andrews *et al.*, “Singular Value Decompositions and Digital Image Processing”, *IEEE Transactions on Acoustics, Speech and Signal Processing*, 1976.
- [28] M. Tanter *et al.*, “Time Reversal and the Inverse Filter”, *Journal of the Acoustical Society of America*, 1, 2000.
- [29] We would like to acknowledge our collaborators from Lincoln Laboratories: Lalitha Parmasewaran and Michelle Clark. We would like to thank MIT Lincoln Laboratories for financial support.
- [30] We would like to thank Jun Xu for performing some of the simulations in this thesis.
- [31] G. Lerosey *et al.*, “Focusing Beyond the Diffraction Limit with Far-field Time Reversal”, *Science*, 315, 2007.
- [32] S. M. Popoff *et al.*, “Measuring the Transmission Matrix in Optics: An Approach to the Study and Control of Light Propagation in Disordered Media”, *Physical Review Letters*, 104, 2010.
- [33] F. Lemoult *et al.*, “Wave Propagation Control at the Deep Subwavelength Scale in Metamaterials”, *Nature Physics*, 9, 2012.

[34] F. Lemoult *et al.*, “Revisiting the Wire Medium: An Ideal Resonant Metalens”, *Waves in Random and Complex Media*, 21, 2011.

[35] We would like to thank Nick Boechler for sharing his expertise on experimental acoustics.

[36] A. Oppenheim and R.W.Schafer, “Digital Signal Processing”, Prentice Hall, 1975

[37] www.physicsclassroom.com

[38] A copy of the raw data is stored in the workstation of our research group.

Appendix

5.1. Operational Conditions of Devices

Table 2 Operating Conditions of the Devices Used in the Acoustic Focusing Experiments

	Properties
Function Generator	
Frequency	60.5 KHz
Amplitude	1 V _{pp}
Type of Signal	5 pulses of sine waves
Filter	
High Pass	Not connected
Low Pass	99.9 KHz
Input Gain	20 dB
Output Gain	20 dB
Amplifier	
Gain	x 10
Offset	+ 50V DC
Translational Stage	
Distance moved between each scanning point	3.75 mm so that hydrophone makes a measurement on top of each resonator hole